Nano Research

Open Access

Review Article

Recent achievements and challenges of large-area and flexible transparent conductive films

Ziqi Zhang[1], Ruiqin Tan[2]✉, Jia Li[1], and Weijie Song[1]✉

[1] *Ningbo Institute of Materials Technology and Engineering, Chinese Academy of Sciences, Ningbo 315201, China*
[2] *Faculty of Electrical Engineering and Computer Science, Ningbo University, Ningbo 315211, China*

Cite this article: *Nano Research*, **2026**, *19*, 94908463. https://doi.org/10.26599/NR.2026.94908463

ABSTRACT: The field of flexible transparent conductive films (FTCFs) has been the subject of extensive research and development over the past decades, especially due to the explosive growth of flexible electronics. Laboratory research has developed a series of novel materials with remarkable performance, yet a significant gap remains between the academic breakthroughs and widespread industrial application, mainly owing to the systemic disconnect between lab conditions and the requirements of industrial-scale production. This review provides a comprehensive, application-driven requirement summary of FTCF technologies, analyzing status on large-area production technologies and key breakthroughs on materials and properties, identifying the critical bottlenecks impeding practical application, and suggesting strategies for future research and industrial development.

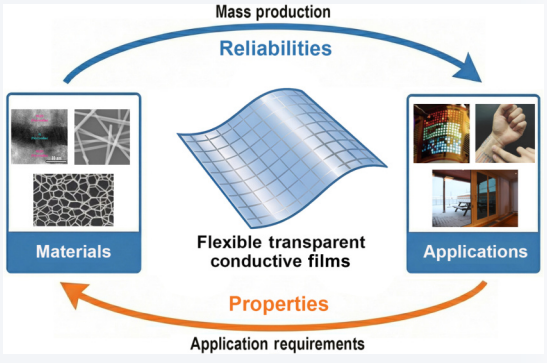

KEYWORDS: flexible transparent conductive films, flexible electronics, large-area fabrication, roll-to-roll, magnetron sputtering

1 Introduction

Flexible transparent conductive films (FTCFs) are foundational components for flexible and wearable electronics [1–4]. The combination of high optical transparency and excellent electrical conductivity makes them a must for foldable displays, smart windows, wearable sensors, and flexible photovoltaic devices [5–10]. It is worth noting that the definitions of "flexibility" are rapidly evolving with divergent application requirements. While traditional flexibility denotes the ability to withstand one-dimensional bending stress, next-generation wearable electronics demand the ability to sustain repetitive multi-directional tensile strains without structural or electrical failure. Furthermore, large-area applications require conformability to arbitrary 3D surfaces. Consequently, the advent of these technologies necessitates novel transparent electrodes capable of withstanding complex mechanical stress without compromising their performance. Many novel materials and fabrication methods have been developed in research laboratories, including silver nanowires (AgNWs), silver meshes, carbon nanotubes (CNTs), graphene, etc. Some of these candidates have demonstrated impressive sheet resistance, optical transmittance, and mechanical flexibility, rivaling or even surpassing those of traditional indium tin oxide (ITO). However, a disproportionately small number of these innovations have successfully transitioned into mass production. A significant gap still exists between these academic breakthroughs and widespread industrial applications. This disconnect arises because laboratory-scale optimization often prioritizes peak performance parameters while neglecting the systemic constraints of industrial production, such as process scalability, batch-to-batch reproducibility, long-term reliability, and total cost of ownership.

There have been several comprehensive reviews of transparent conductive materials categorizing technologies by material class, such as metal oxides, carbon-based materials, metal nanowires, ultra-thin metal films, metal meshes, and conductive polymers [11–17]. While this approach is valuable for mapping the scientific landscape of FTCFs, it fails to capture the market demands and multifaceted challenges of commercialization.

Here, this review adopts an alternative, application-driven framework to bridge the gap between new materials and industrial production. The review first elaborates the specific performance requirements of key end-use applications, including touchscreens, heaters, electromagnetic interference (EMI) shielding, smart

Received: November 30, 2025; **Revised:** January 17, 2026
Accepted: January 20, 2026

✉Address correspondence to Ruiqin Tan, tanruiqin@nbu.edu.cn; Weijie Song, weijiesong@nimte.ac.cn

windows, photovoltaics, and electronic skins. The analysis of practical requirements can critically assess how existing and emerging FTCF technologies either meet or fall short of these commercial benchmarks. Subsequently, the review focuses on the issues of substrate selection, roll-to-roll (R2R) processing, and cost evaluation in scalable manufacturing, revealing the pathway and roadblocks in mass production. It then demonstrates the recent progress in material optimization and structural design of FTCFs. To clearly assess the proximity of different FTCF technologies to practical applications, the manufacturing readiness level (MRL) framework is also introduced to quantitatively evaluate the industrial maturity. Finally, through matching material performance with practical application requirements, the review points out several bottlenecks that urgently need to be addressed for FTCFs. By clarifying the specific gaps between current academic achievements and industrial requirements, this review aims to guide the development of FTCFs toward more commercially viable pathways.

2 Application trends and requirements of large-area flexible transparent conductive films

2.1 Touchscreens

Since the development of ITO deposition on polymeric films in the late 1970s, ITO/polyethylene terephthalate (PET) films have emerged as one of the leading commercial product successes for the sputter roll coating industry, particularly driving the growth of projected capacitive touch sensor market [18, 19]. In the field of large-sized touchscreens, although infrared touchscreens demonstrate distinct cost advantage, they require raised bezels and are susceptible to interference from strong ambient light or dust [20]. Conversely, projected capacitive touchscreens support bezel-less and curved designs, thereby securing a growing share of the market. The adoption of FTCFs is strictly necessary to transcend the limitations of flat surfaces, as the performance of modern projected capacitive touchscreens is intrinsically linked to the electrical properties of the FTCFs. As touchscreen size increases, the required sheet resistance of the FTCFs must decrease significantly to below 10 Ω/sq to maintain functionality, speed, and accuracy [21]. With excellent transparency but a relatively high sheet resistance (< 50 Ω/sq), ITO/PET films dominate the small-screen market, where the resistance-capacitance (RC) delay and the signal-to-noise ratio (SNR) are manageable. However, as screen size increases, performance drops dramatically as resistance increases, making ITO unsuitable for large-area applications [22]. Furthermore, the films must keep high optical transmittance (> 90%) with minimal haze (< 1%) and suppress the formation of visual artifacts that could interfere with the underlying display [23]. Additionally, a low surface roughness (< 10 nm) is required to prevent short circuits caused by the penetration through the dielectric layer. For emerging applications such as foldable smartphones, the films are further required to withstand hundreds of thousands of folding cycles at a bending radius of 1–2 mm. Compatibility with scalable, low-cost manufacturing methods, such as printing technologies and R2R processing, is vital for the economic production of large flexible sensors [24]. Products based on AgNWs, metal meshes, and ultra-thin metal films have been demonstrated as solutions specifically to address the low-resistance requirements of larger screens [12, 25–27]. These technologies can achieve sheet resistance values an order of magnitude lower than that of ITO while maintaining acceptable optical properties, making them indispensable for large-format touch displays. Recent products from FlexTouch reported that the Cu mesh touch sensors revealed higher SNR, better bending, higher transmittance and better response than ITO-based sensors because of the use of low sheet resistance materials. Typical commercially available AgNWs-based touch sensors also revealed short response time and high transmittance with size up to 110 inches. There have been reports on CNTs, conductive polymers, and graphene-based touch screens, but with only limited commercial success [13, 28, 29].

2.2 Transparent heaters (THs) and EMI shielding

Transparent and flexible films that provide both heating and EMI shielding are getting increasing attention owing to their diverse practical applications in complex electronic systems. In automotive, radar, and aerospace applications, THs are essential for de-icing, defogging, and thermal stabilization of windshields, cockpit displays, and critical camera/sensor lenses, ensuring visibility and proper electronic function in extreme cold [8]. Concurrently, integrated EMI shielding in these same systems protects sensitive onboard electronics from external and internal electromagnetic radiation, which is critical for safety and compliance to military and aerospace standards [9, 30]. Beyond transportation, these multifunctional films are used for all-weather visibility in outdoor kiosks and ATMs [31], and in specialized medical and laboratory equipment for temperature control [32]. There is an inherent trade-off in the material design, as the required increase in conductivity for effective EMI shielding and rapid heating (often achieved by increasing nanowire density) can reduce the crucial visible light transmittance (transparency) and increase optical haze [33, 34]. In addition, localized hotspots might be a problem due to inhomogeneous current, which may decrease the device lifetime. This led to the development of hybrid composites with materials like CNTs to resolve these stability and uniformity issues [35, 36].

2.3 Smart windows

The global market for smart windows, including windows with polymer-dispersed liquid crystal (PDLC) devices, suspended particle (SPD) devices, and electrochromic (EC) devices, is undergoing a period of accelerated expansion primarily fueled by synergistic demands from the architectural and automotive sectors [6]. In architecture, growth is mainly driven by the global trend toward green building certifications, which requires superior energy efficiency. Accordingly, electrochromic devices dominate this application due to their capacity to dynamically regulate the solar heat gain coefficient and visible light transmission, thereby significantly reducing the operational electricity load [37]. Driven by the focus on passenger experience, electrochromic devices are also one of the fastest-growing parts for automobiles, as their rapid switching speed is crucial for instantaneous privacy and glare control in panoramic roofs [38]. Crucially for electric vehicles, the thermal regulation provided by smart glass reduces the energy drain from the air conditioning system, which directly contributes to extended battery range [39]. The smart glass also facilitates the integration of advanced driver-assistance systems and augmented reality heads-up displays into the functional "smart windshield". All the above-mentioned flexible devices use two pieces of FTCFs [40–42], which brings a fast boost on commercial demands. Table 1 gives typical parameters of these devices and typical properties of

the required FTCFs. It is worth noticing that these parameters depend strongly on the size of devices. Especially for electrochromic devices with a driving voltage of only several volts, the ohmic loss through a large area is a key factor limiting the device speed and homogeneity [43–45].

2.4 Flexible photovoltaics

Traditional thin film solar cells, especially copper-indium-gallium-selenium technologies, use transparent and conductive flexible polyimide substrates mostly for space applications where weight, durability, and flexibility are fatal parameters [46]. Ascent Solar was the only supplier, mainly due to the production difficulties and market scale of the products. Flexible organic photovoltaics (OPV) is a newer technology known for being ultra-lightweight, semi-transparent, and highly flexible. Besides traditional ITO films, conductive polymers based FTCFs, specifically poly(3,4-ethylenedioxythiophene):polystyrene sulfonate (PEDOT:PSS), are adopted for the R2R manufacturing of OPV in companies like Heliatek [47]. Commercial solutions also include "FineX" conductive mesh films provided by Panasonic and "Ag-stacked film" provided by TDK for OPV applications. All these thin films demonstrated not only low sheet resistance but also high bendability which are highly desired for flexible applications [16, 48, 49]. Novel studies on carbon-based FTCFs and polymer composite-based FTCFs are still in research level [50–53].

2.5 Electronic skins

Other than the above-mentioned flexible electronic devices, stretchable tactile sensors, or "e-skin", for humanoid robots are advancing rapidly, moving beyond simple pressure sensing to become a critical component for safe and dexterous interaction [7]. It represents the transition from robots that simply look human to robots that can feel the world like humans. The field is currently experiencing a rapid convergence of materials science, 3D printing, and artificial intelligence, moving breakthroughs from the lab toward practical application [54–56]. Current e-skin research focuses on creating multifunctional, durable, and large-area skins capable of intelligent signal processing [57–59]. To achieve conformability on complex 3D surfaces, the FTCFs designed for e-skins employ emerging solutions such as geometric engineering and elastic composites [60, 61]. These strategies enable the electrodes to preserve electrical conductivity even under significant multi-directional tensile strains. Despite successes in research, a humanoid robot fully covered in high-fidelity e-skin is not yet a commercial reality due to several critical challenges. The complex micro-fabrication processes that work in the lab are prohibitively expensive and difficult to scale to cover the entire surface of a robot. Reproducibility and cost-effectiveness for mass production remain elusive [10]. Given that a functional robot will inevitably scrape, bump, and wear down its skin, the fragility and sensitivity of most current e-skins to mechanical stress and environmental conditions remain a critical challenge, despite that self-healing materials are promising [62]. Furthermore, linking and powering millions of flexible sensors to a central processor is also a challenge [63]. The operation of vast sensor arrays requires a constant power supply, making batteries an unsustainable solution for mobile robots. This limitation is pushing research toward integrated energy harvesting, which is still in its early stages [64].

2.6 From application requirements to material selection

As summarized in Fig. 1, different applications exhibit distinct requirements for FTCFs. Touchscreens necessitate high optical clarity and touch sensitivity. Thus, FTCFs in touchscreens require a sheet resistance below 10 Ω/sq to minimize RC delay, along with a transmittance exceeding 90% and haze below 1% to ensure display brightness and clarity. Transparent heaters prioritize fast and uniform heat dissipation, imposing strict requirements on the thermal conductivity. Furthermore, excellent thermal stability of FTCFs is essential to withstand prolonged operation at elevated temperatures. For EMI shielding applications, high electrical conductivity is the primary consideration, followed by the capability to reflect electromagnetic waves over a broad frequency range. In smart windows, low sheet resistance is vital for improving switching speeds. Additionally, FTCFs must possess robust chemical stability to endure ion migration processes, particularly in electrochromic devices. Flexible photovoltaics demand high transmittance at the visible range to maximize photon harvesting. Unlike display devices, higher haze is often acceptable or even beneficial here, as it increases the optical path length via light scattering. It should be noted that a low sheet resistance about 20 Ω/sq remains critical in photovoltaics, especially for large-area modules. Regarding e-skins, FTCFs' mechanical properties such as elasticity, stretchability, and fatigue resistance are of primary importance. Additionally, excellent biocompatibility is required for direct human-contact applications. In summary, the properties of FTCFs must be tailored to meet specific application demands, since simultaneously optimizing all properties is not a feasible strategy.

3 Issues of the mass production of flexible transparent conductive films

3.1 Flexible substrates

The transition from laboratory-scale prototypes to commercially viable FTCF products is governed by the constraints of high-throughput manufacturing. Substrate selection constitutes the first

Table 1 Key device parameters and requirements of FTCFs for smart window applications

Types of smart window	PDLC	SPD	EC
Main function	On-demand privacy	Dynamic tinting, glare/heat control	Dynamic tinting, energy conserving
Default state	Opaque	Dark	Previous state (bi-stable)
Active state	Transparent	Transparent	Changes state (tints or clears)
Switching speed	Very fast	fast	Slow to fast
Sheet resistance	< 200 Ω/sq	< 200 Ω/sq	< 20 Ω/sq
Light transmittance	> 85%–92%	> 80%–90%	> 70%–90%
Required durability & flexibility	Chemically/thermally stable, on flexible substrates	Chemically/thermally stable, on flexible substrates	Chemically stable against the electrolyte, flexibility is a challenge

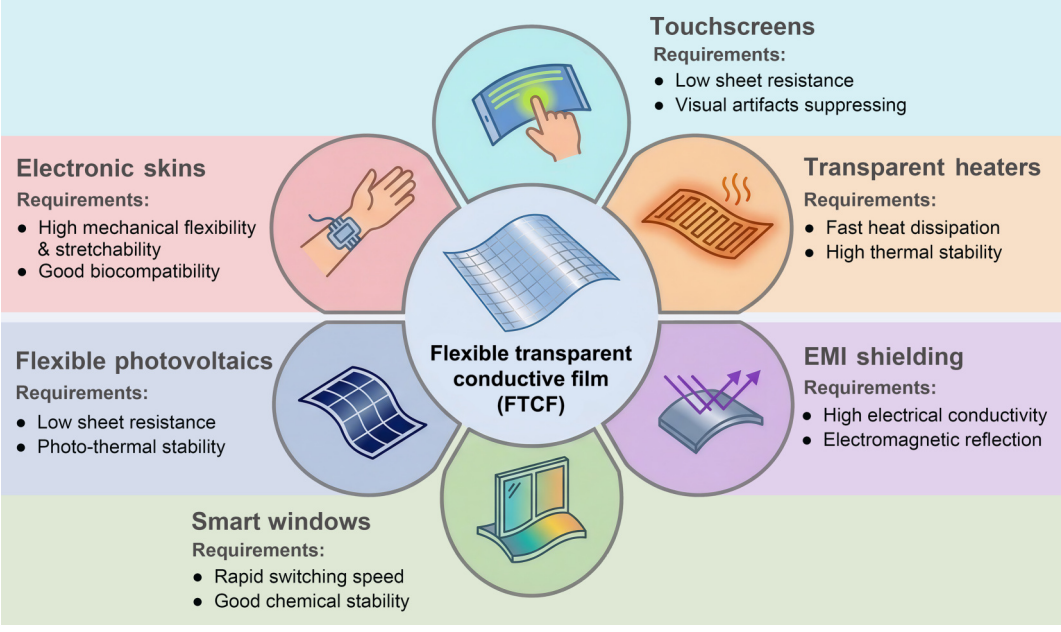

Figure 1 Summary of different applications and corresponding requirements for FTCFs.

step in this process, as it dictates the thermal and mechanical limits of following deposition and ultimately constrains device performance and reliability. Although polymer substrates inherently provide mechanical flexibility, industrial applications require materials that function as fully engineered components [65]. In FTCF industry, PET substrates used are mainly "heat-stabilized" biaxially oriented (BOPET) grades [66]. These are essential for maintaining dimensional stability during high-temperature vacuum deposition processes [67]. Unlike standard packaging-grade films, optical-grade PET substrates intended for R2R magnetron sputtering go through a post-stretching thermal relaxation process. This process relieves residual internal stresses and reduces thermal shrinkage to below 0.3% (machine direction/transverse direction) after exposure to 150 °C for 30 min [68]. Such low shrinkage is critical for touch applications, especially those using flexible ITO. The semi-crystalline PET exhibits a roughness of approximately 15–30 nm due to anti-blocking particles added for winding mechanics [69]. However, high-quality conductive oxide films require a smooth nucleation surface to minimize variations in sheet resistance and prevent open-circuit defects. Therefore, commercial transparent-conductive-film-grade PET always comes with a pre-applied, UV-cured acrylic or siloxane-based planarization layer (hard coat), which not only smooths the surface but also acts as a diffusion barrier for low molecular-weight oligomers [70, 71]. These oligomers, primarily cyclic trimers inherent to PET polymerization equilibrium, diffuse to the surface at temperatures above 110 °C and crystallize into white particulate defects, which break the continuity of nanoscale conductive coatings and increase optical haze [72, 73]. Optically, these engineered PET substrates achieve a total transmission of 88%–92%, with haze levels maintained below 0.6%–1.0% [74–76].

By replacing the terephthalate unit in PET with a double naphthalene ring, polyethylene naphtholate (PEN) films exhibit significantly higher glass transition temperatures (T_g) and Young's modulus [77, 78]. This improved thermal stability is particularly valuable for applications such as perovskite solar cells, which require heating during crystallization procedures [79]. Furthermore, PEN demonstrates superior intrinsic barrier properties. Its water vapor transmission rate (WVTR) and oxygen transmission rate (OTR) are approximately 3 to 5 times lower than those of PET, owing to the denser molecular packing of the naphtholate moiety [80–83]. This reduces the dependency on secondary encapsulation layers in sensitive organic electronic devices. Typical PEN film products, such as the Teonex® series (specifically grade Q65FA) by Teijin DuPont Films, are engineered with surface pre-treatments similar to optical PET to control surface roughness and oligomer migration. However, the cost of such films is typically 4 to 5 times higher than that of PET, which limits their commercial application.

Colorless polyimide (CPI) is the most expensive commercial available substrate for FTCFs. It is specifically engineered to overcome the thermodynamic and mechanical limits of polyesters such as PET and PEN, while also avoid the parasitic absorption typical of aromatic polyimides [84]. To achieve high optical transparency (total transmission > 88%–90% and yellow index < 3.0), the CPI polymer backbone is synthetically modified via the incorporation of electron-withdrawing substituents (e.g., trifluoromethyl groups) or alicyclic structures (e.g., cyclohexane) [85, 86]. These modifications prevent the formation of intra- and intermolecular charge-transfer complexes that absorb blue-violet photons [87]. This molecular design gives CPI an exceptionally high T_g above 300 °C [88, 89], allowing it to endure harsh high-temperature processing, such as the annealing of indium gallium zinc oxide (IGZO) thin-film transistors or the crystallization of ultra-low resistance ITO [90, 91]. Under these conditions, PET would suffer catastrophic thermal degradation. Mechanically, CPI films exhibit superior fatigue resistance, maintaining structural integrity through hundreds of thousands of dynamic folding cycles at radii below 1–2 mm [92, 93]. However, its pristine polymer surface is relatively compliant (pencil hardness ~ HB) and generally requires a siloxane-based hybrid hard coat to provide sufficient abrasion resistance for use as exterior display cover windows [94, 95]. Based on the above discussion, the properties and key advantages/disadvantages of different flexible substrates are summarized in Table 2.

Table 2 Properties and key advantages/disadvantages for flexible substrates

Materials	PET	PEN	CPI
T_g (°C)	~ 80	~ 120	> 300
Optical transmittance	88%–92%	87%–88%	88%–90%
WVTR (g/(m²·day))	1.4–3	0.5–1.3	0.2–3
Surface properties	Rough surface	High Young's modulus	Soft surface
Relative cost	Low	High	Very high
Key advantage	Cost-effective	Superior barrier properties	Thermal and folding stability
Key disadvantage	Failure at high temperature	High price	Requires surface hardening

3.2 Roll-to-roll processing

The industrial-scale fabrication of FTCFs is predominantly implemented using R2R platforms to meet high-throughput requirements. Multiple deposition technologies can be integrated into R2R architectures, and key manufacturing metrics—including throughput, yield, reproducibility, and total cost of ownership—are governed by the underlying deposition mechanisms and material properties. As a result, different FTCF material systems impose distinct process constraints and optimization challenges.

Flexible ITO films are primarily produced via R2R magnetron sputtering (Fig. 2(a)), a process that requires a complex optimization to balance the physical limitations of thin-film growth with high-volume manufacturing [96]. The physics of reactive sputtering and the thermal constraints of polymeric substrates are both critical determining factors [97, 98]. In R2R systems, production throughput depends not merely on web speed but also on the dynamic deposition rate and the maximum permissible thermal load on the substrate [98]. Modern high-throughput lines utilize rotatable magnetrons instead of planar cathodes which allow for significantly higher power densities (up to 20–30 kW/m) [99, 100], and thus higher sputtering rates can be achieved without melting the target bonding or overheating the substrate, provided that the web is kept in intimate thermal contact with a precision-cooled coating drum (typically maintained at −10 °C to 20 °C). Throughput can be further scaled by arranging multiple cathodes in series within the deposition zone [101]. However, this increases the complexity of gas distribution, as each cathode requires a localized gas environment to maintain uniformity [102]. Yield losses in R2R ITO sputtering are frequently attributed to micro-arcing and particulate generation. As the target material erodes, insulating oxide patches can form on the target surface. These patches accumulate charge until a dielectric breakdown occurs, resulting in an arc that ejects macro-particles onto the moving web and creates pinhole defects [103, 104]. To mitigate this issue, pulsed DC or middle-frequency AC power supplies (20–100 kHz) are employed [105–107]. These power sources periodically reverse the voltage polarity at the target, discharging the accumulated positive ions on the insulating regions before an arc can form [108, 109]. Furthermore, water vapor desorption during sputtering incorporates hydrogen and hydroxyl groups into the ITO lattice, which may significantly influence film conductivity [110–112]. Therefore, high-yield lines require sophisticated pumping architectures, including differentially pumped unwinding chambers and cryogenic (Meissner) traps to capture water vapor before it reaches the process zone [98, 113]. Commercial flexible ITO production lines are available from companies such as Applied Materials and ULVAC Inc., with typically price of multi-million US dollars and dynamic deposition rate of several meters per minute. These production lines can also be optimized to produce oxide/metal/oxide (OMO)-structured FTCFs since they share the same multi-layer nanofilm structure [114–117].

In contrast to vacuum-based processing, R2R solution processing serves as another essential mass production technique, as shown in Fig. 2(b) [118]. A typical example is the fabrication of AgNW-based FTCFs, in which the deposition of a thin, uniform liquid film onto a moving web presents a complex physical process. This process is governed by the interaction of viscous, capillary, and inertial forces [119–121]. Slot-die coating is widely regarded as the premier technique for fabricating high-performance FTCFs due to its pre-metered nature [122–124]. As the ink passes through the slot gap, the existing shear field can induce orientation of high-aspect-ratio particles such as AgNWs. Computational fluid dynamics modeling suggests that high shear rates in the slot align nanowires parallel to the flow direction [125]. While this alignment can enhance conductivity along the machine direction, isotropic conductivity is usually desired. Therefore, process engineers must balance the shear rate (via gap height and flow rate) to minimize excessive anisotropy while ensuring flow stability [126]. The "ink" is not a simple carrier but a sophisticated functional fluid engineered to navigate the hydrodynamic stresses of the coating process. Here, solvent selection is critical, as it governs drying rate and surface tension [127–129], and solvent recycling is one of the key processes for controlling production costs. Additionally, dispersions containing AgNWs typically require a polymeric binder, which creates a viscoelastic matrix that anchors the nanowires to the substrate and to each other [130]. Once the liquid film is deposited, it must be transformed into a solid, conductive network through drying and sintering. Drying in R2R lines is typically done in hot-air impingement tunnels [131, 132], where the rate of solvent evaporation defines the final film morphology. As-deposited AgNWs networks exhibit high resistance due to the insulating polyvinylpyrrolidone (PVP) ligand shell and the poor physical contact at their junctions [133]. Sintering is the crucial process of welding these junctions to form a true metallic continuum. Among various techniques, photonic sintering has emerged as an enabling technology for high-speed R2R processing of AgNWs [134, 135]. Alternatively, cold sintering methods employing chemical agents exhibit unique attractiveness for ultra-sensitive substrates. For example, exposure to chloride ions or specific polymer overcoats can dissolve the PVP shell and promote Ostwald ripening at the nanowire junctions, fusing them at room temperature [136]. While the total cost of ownership for AgNWs-based FTCFs benefits from the elimination of high-vacuum infrastructure and the low areal mass density of silver (~ 50–100 mg/m²) [137], realizing this economic advantage depends on mastering the encapsulation of the nanowires. Proper encapsulation is essential to prevent

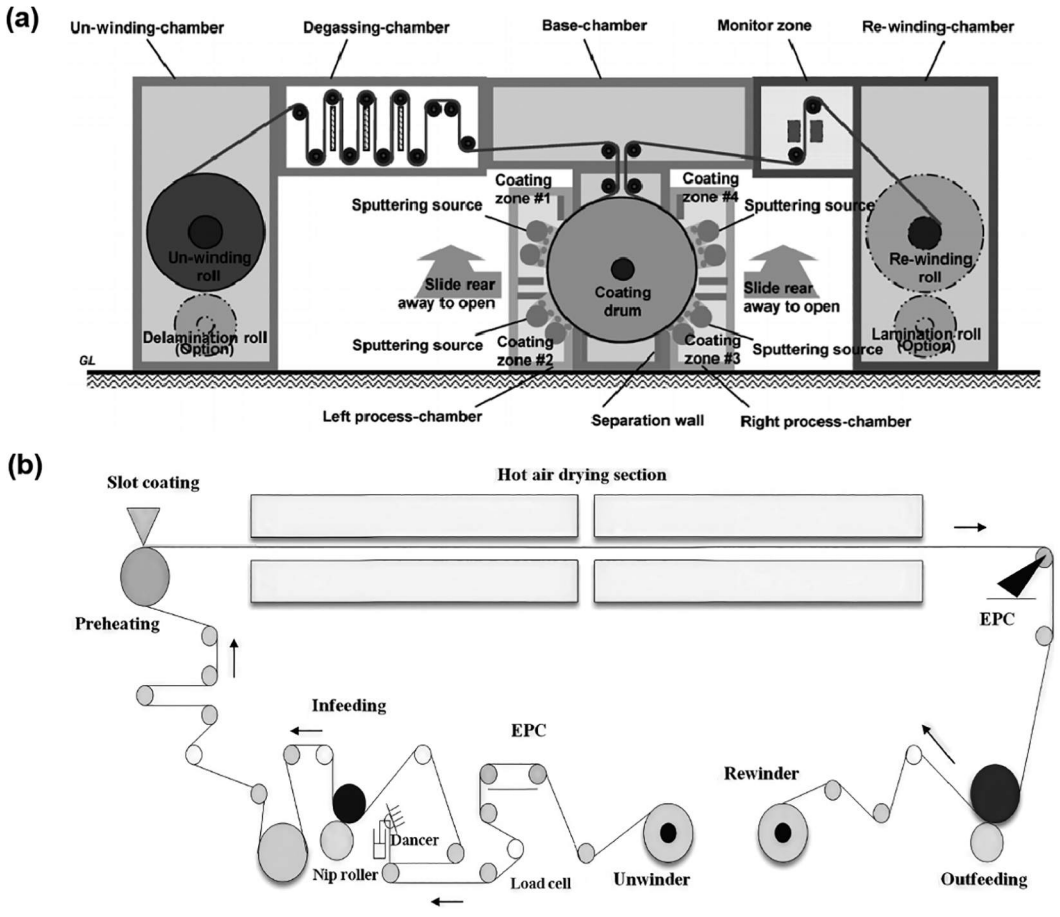

Figure 2 (a) Schematics of roll-to-roll sputtering systems. Reproduced with permission from Ref. [96], © Kobe Steel, Ltd. 2016. (b) Schematics of roll-to-roll slot-die coating systems. Reproduced with permission from Ref. [118], © Elsevier Ltd. 2014.

environmental sulfidation and electromigration, as these phenomena remain the primary failure modes in real-world applications [138, 139].

3.3 Cost evaluation

Overall, the cost of FTCF manufacturing emerges from the coupled influences of substrate selection, deposition methodology, capital investment, throughput, and yield. It is worth noting that although some FTCFs have been commercially available, estimating their manufacturing costs based on market prices remains difficult. This is largely due to the prevalence of captive production, where major manufacturers integrate the production of both raw materials and end-products internally. This vertical integration of the supply chain obscures the standalone cost of the FTCFs. A comparative summary of the relative costs associated with different FTCF material systems is presented in Table 3.

Flexible ITO dominates the FTCF market and therefore serves as a practical baseline for cost comparison. Its high material and equipment costs arise primarily from indium consumption and the need for high-vacuum sputtering infrastructure. However, the maturity and throughput of R2R sputtering lines largely offset these initial expenses, resulting in a total cost of ownership that remains acceptable for many commercial applications [140]. In contrast, AgNW-based FTCFs can be produced using solution-based methods that reduce capital investment and support high manufacturing speeds. For these systems, the principal cost constraint is the intrinsic price of silver. Copper-mesh electrodes provide a substantial material-cost advantage over AgNWs while achieving comparable electrical performance [45], and they can be fabricated using high-throughput processes such as printing or wet etching [141, 142], yielding significantly lower overall costs than ITO. Carbon-based conductors, including CNTs and graphene, benefit from low raw material costs. However, solution-processed CNTs and reduced graphene oxide (GO) suffer from dispersion

Table 3 Relative cost analysis for different FTCF material systems

Materials	ITO	AgNWs	Metal mesh	CNT	Graphene (CVD)
Material cost	High	High	Medium	Low	Low
Equipment cost	High	Low	Low	Low	High
Production speed	High	High	High	Medium	Low
Yield	High	Medium	Medium	Low	Low
Estimated total cost	Medium	Medium	Low	High	Very high

instability and generally inferior electrical performance compared with metal-based counterparts [143], resulting in relatively high total costs despite inexpensive precursors. Conversely, chemical-vapor-deposition-grown (CVD-grown) graphene offers superior electrical properties but depends on costly vacuum deposition equipment and requires a transfer step that limits throughput and reduces yield [144]. As a result, the overall cost of high-quality CVD graphene remains prohibitive for most large-area applications.

Based on the market data of 2024, the market size for FTCFs is valued at approximately USD 3.83 billion, accounting for nearly 60% of the total transparent conductive film market. In terms of material composition, ITO on PET substrates currently retains a dominant position, holding approximately 40%–50% of the flexible market share, predominantly in small-area and low-end applications. This significant share is largely attributed to the well-established manufacturing infrastructure in the flat panel display industry. However, owing to their low sheet resistance and lower equipment cost, AgNWs and metal meshes have rapidly captured the majority share in high-end foldable display applications. Notably, Chinese enterprises such as Huake Tek and Nuovo Film have emerged as primary global suppliers of AgNWs, outpacing major competitors in Japan and the United States during this growth phase. Additionally, FlexTouch and Ofilm have successfully commercialized advanced metal mesh technology, achieving full localization of the supply chain within China. The market share of these non-ITO materials is projected to reach 60%–70% by 2030.

4 Material considerations and optimization methods for flexible transparent conductive films

4.1 Silver nanowires

The electrical conductivity of AgNWs is mainly controlled by the intrinsic conductivity of individual nanowires and the contact resistance at wire-to-wire junctions. According to the percolation theory, the AgNWs network tends to become much more conductive once the nanowire density surpasses a percolation threshold [145]. Increasing the nanowire length significantly reduces the number of junctions to form a continuous conductive network, thereby lowering the percolation threshold. This allows for high conductivity at a lower material density, which directly benefits optical transmittance. Conversely, the nanowire diameter primarily determines the light scattering cross-section. Thinner nanowires exhibit improved optical transmittance and suppressed haze, but with a reduction in intrinsic conductivity. To balance this trade-off, maximizing the aspect ratio serves as the key strategy for achieving low sheet resistance simultaneously with high transmittance in AgNW-based FTCFs. The geometric dimensions (length and diameter) of the nanowires can be controlled during synthesis. For instance, high-aspect-ratio AgNWs can be obtained via the polyol method by optimizing the concentration of $AgNO_3$ and the addition of Cl^- ions (Fig. 3(a)) [146, 147]. Bleiji et al. fabricated an ultra-long AgNW grid though a bottom-up electrochemical growth method , achieving a low sheet resistance of 3.7 Ω/sq at 95.9% transmittance [148]. Reducing junction resistance primarily relies on welding processes. Various post-treatment methods, such as photonic sintering, chemical welding, and capillary-induced cold welding, have been applied, in consideration of the thermal tolerance of the substrate [134–136, 149]. As shown in Fig. 3(b), Jiang et al. reported efficient welding using $Ti_3C_2T_X$ MXene nanosheets, producing an electrode of 13.9 Ω/sq and 83.8% transmittance [150]. In terms of mechanical stability, the degradation of optoelectronic performance in AgNW-based FTCFs under repetitive bending often results from crack formation in the conductive layer or delamination from the substrate. Kim et al. introduced polyurethane–urea (PUU) to enhance the adhesion between AgNWs and a poly(dimethylsiloxane) (PDMS) substrate (Fig. 3(c)) [151]. The AgNWs/PUU/PDMS electrode exhibited high

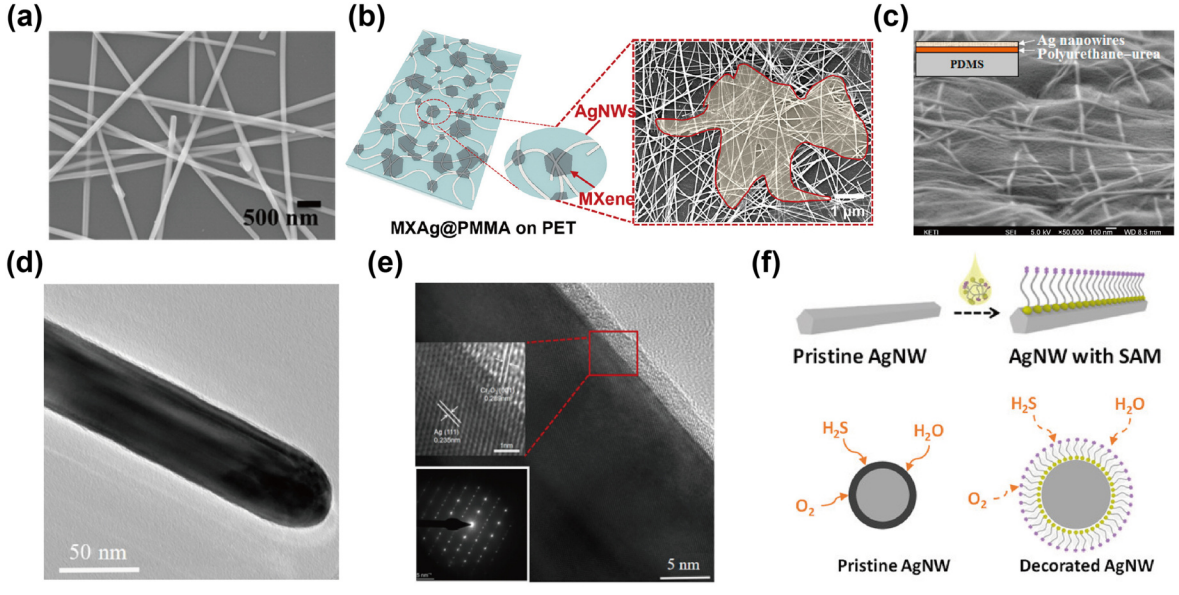

Figure 3 (a) Scanning electron microscopy (SEM) image of AgNWs synthesized with optimal $AgNO_3$ concentration. Reproduced with permission from Ref. [147], © Elsevier B.V. 2015. (b) Schematics and SEM image of the MXene-AgNWs embedded in poly(methyl methacrylate) (MXAg@PMMA) electrode. Reproduced with permission from Ref. [150], © American Chemical Society 2022. (c) SEM image of the AgNWs/PUU/PDMS film. Reproduced with permission from Ref. [151], © American Chemical Society 2015. (d) High-resolution transmission electron microscopy (HRTEM) and (e) high-angle annular dark-field scanning transmission electron microscopy (HAADF-STEM) images of Ag/Cr_2O_3 NW. Reproduced with permission from Ref. [154], © American Chemical Society 2023. (f) Schematics of the surface modification and shield effect of the MBI molecule. Reproduced with permission from Ref. [155], © American Chemical Society 2018.

stability, withstanding 100 stretching-releasing cycles at 50% strain. Regarding chemical stability, AgNWs are susceptible to sulfidation when exposed to hydrogen sulfide and carbonyl sulfide in the ambient air [152]. Their high specific surface area accelerates this corrosion process. Depositing metals such as Ni or Pd onto AgNWs to form core–shell metallic networks can mitigate this issue [153]. This strategy not only improves corrosion resistance but also allows tuning of the surface work function, enhancing its performance in the OLED devices. Figures 3(d) and 3(e) demonstrate a high-quality core–shell structural Ag/Cr_2O_3 NW with uniform Cr_2O_3 coverage [154]. The modified AgNWs-based films exhibited good oxidation resistance, thermal stability, and mechanical flexibility, with minimal loss in the conductivity and transmittance of the original AgNW network. Furthermore, Liu et al. employed 2-mercaptobenzimidazole (MBI) molecules, which chemisorbed onto AgNW surfaces via strong Ag–S bonds, forming a hydrophobic shield, as shown in Fig. 3(f) [155]. The MBI-treated AgNWs demonstrated enhancement in antioxidation and antisulfidation, along with ultra-high thermal stability up to 400 °C.

4.2 Metal mesh

The optoelectronic performance of metal mesh electrodes is primarily determined by their structural design and fabrication precision. By carefully controlling geometric parameters such as line width and pitch, an optimal balance between transparency and conductivity can be achieved [156, 157]. High-precision patterning techniques, such as photolithography and nanoimprint lithography, have been employed to ensure fine and well-defined mesh structures [158, 159]. To reduce manufacturing costs, Yuan et al. introduced a solution-based two-step surface energy-directed assembly (SEDA) process for efficiently fabricating high-resolution Ag mesh, as illustrated in Fig. 4(a) [27]. Using SEDA, a line width down to 2 μm can be achieved on various substrates, resulting in an Ag mesh with excellent optoelectronic properties of 1.79 Ω/sq and 92% transmittance. As for optical performance, the periodic nature of metal mesh can lead to moiré fringes, especially in touch panel applications. To suppress moiré patterns, researchers have developed random mesh architectures via electrohydrodynamic jet printing (Fig. 4(b)) and the crackle template method (Fig. 4(c)) [141, 160]. Similar to AgNWs, the stability of metal mesh is constrained by silver's susceptibility to sulfidation and copper's susceptibility to oxidation [161]. Therefore, surface encapsulation strategies have been widely adopted. For instance, through a thin poly(1-vinyl-3-ethylimidazolium bis(trifluoromethanesulfonyl) imide) (P[VEIM][NTf_2]) ionogel layer encapsulation (Fig. 4(d)), Chang et al. significantly improved the flexibility and environmental stability of the Cu mesh [162]. Additionally, mechanical stability can be further improved by coating the Ag mesh with AgNWs, as demonstrated by Yang et al., maintaining constant electrical performance over 5000 bending cycles [163].

4.3 Carbon-based materials

Carbon-based materials are promising for FTCFs due to their exceptional chemical stability, mechanical flexibility, and high theoretical carrier mobility for graphene. However, the transfer process of CVD-grown graphene is prone to introducing wrinkles and contamination, thereby reducing conductivity and uniformity [17, 164]. Therefore, optimizing the transfer process is critical in the practical fabrication. Figure 5(a) illustrates a direct R2R transfer process using photocurable epoxy resin, which has been able to fabricate a 100-m-long graphene FTCF with a sheet resistance as low as 150 Ω/sq [165]. Solution-processable CNTs offer a cost-effective alternative, but their conductivity requires further improvement for broader applications. A major challenge lies in dispersing ultra-long CNTs without damage or shortening [28]. Liu et al. developed polythiophene-functionalized CNTs (PMTA-CNTs) to achieve better dispersion without compromising their conductivity [166]. These functionalized CNTs can undergo UV-triggered free-radical polymerization (Fig. 5(b)), forming a 3D cross-linked network that delivers superior flexibility and an electrical conductivity of 1613 S/m. Combing the acid doping method, Zhou et al. find that the assistance of moderate acids can significantly improve the exfoliation of CNTs with negligible structure damage [167]. As shown in Figs. 5(c) and 5(d), the CNT films with H_2SO_4-assisted dispersion exhibit sheet resistances of 75 Ω/sq and 84% transmittance with excellent chemical stability. Furthermore, hybrid

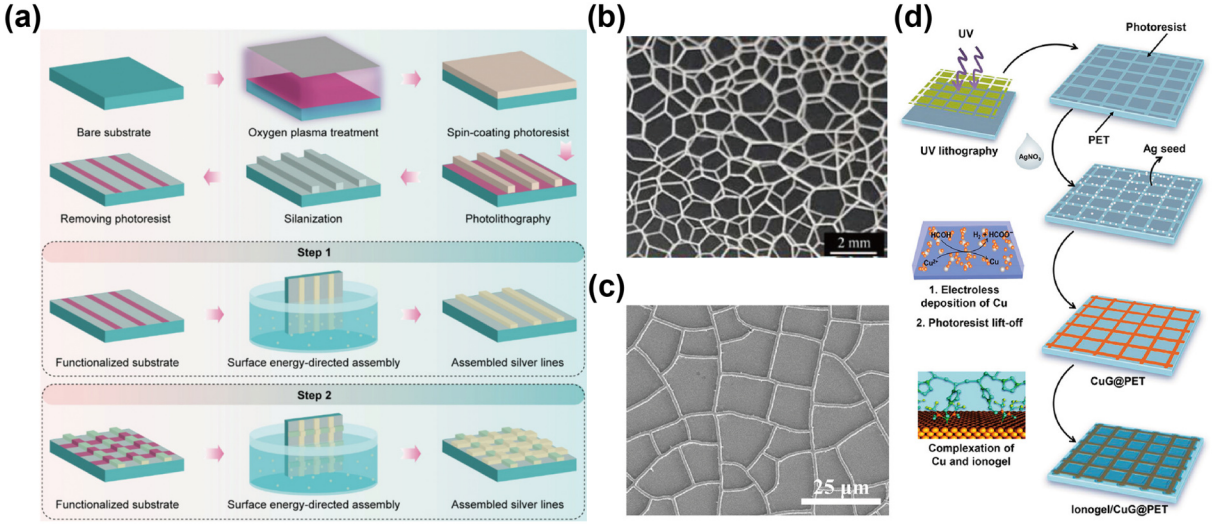

Figure 4 (a) Schematics of the functionalized substrate preparation and the SEDA process for Ag mesh fabrication. Reproduced with permission from Ref. [27], © Yuan, S. Q. et al. 2023. (b) Double-sided random metal mesh pattern fabricated via electrohydrodynamic jet printing. Reproduced with permission from Ref. [160], © Elsevier Ltd. 2022. (c) Copper mesh pattern fabricated via the crackle template method. Reproduced with permission from Ref. [141], © Chen, Z. B. et al. 2024. (d) Schematics of the designing concept and fabrication process for ionogel/Cu grid-based FTCFs. Reproduced with permission from Ref. [162], © American Chemical Society 2018.

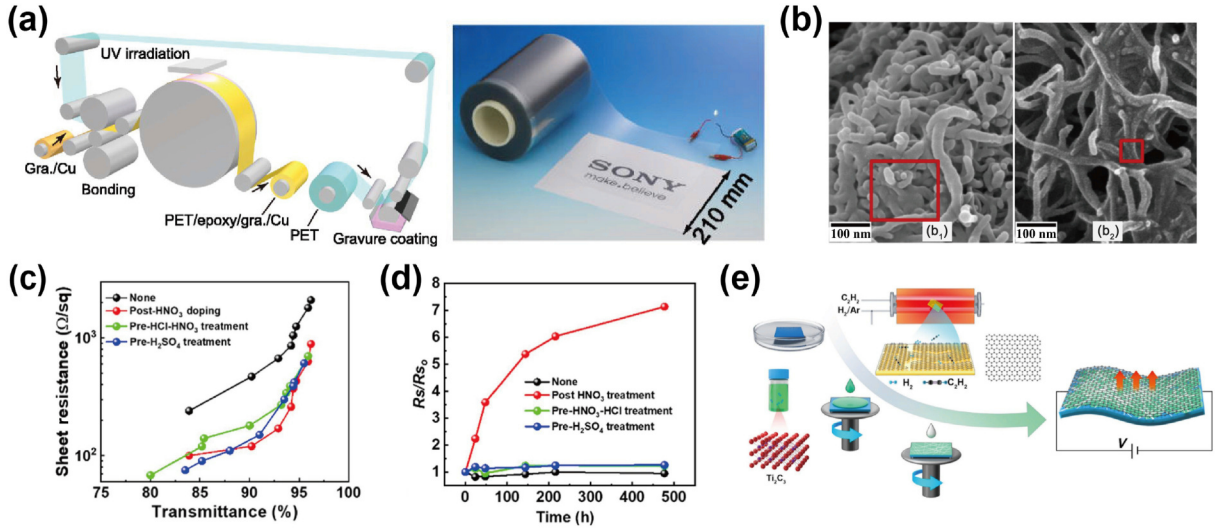

Figure 5 (a) Schematics of the R2R transfer system and the photograph of fabricated graphene FTCFs. Reproduced with permission from Ref. [165], © American Institute of Physics 2013. (b) SEM images of PMTA-CNT coating before and after UV curing, indicating the formation of 3D network. Reproduced with permission from Ref. [166], © Elsevier B.V. 2025. (c) Sheet resistance versus transmittance and (d) sheet resistance variation in damp-heat test of CNT films with different acid treatments. Reproduced with permission from Ref. [167], © Elsevier B.V. 2020. (e) Schematics of the fabrication process of the hybrid MXene/AgNW/graphene FTCFs. Reproduced with permission from Ref. [168], © Elsevier Ltd. 2022.

structures that combine carbon materials with other conductive components compensate for their inherent limitations in conductivity and stability. Wang et al. reported a hybrid FTCF with a sandwiched structure composed of MXene, AgNW, and graphene (Fig. 5(e)) [168]. In this configuration, the bottom MXene layer enhances substrate adhesion, the top graphene layer serves as a protective barrier, and the intermediate AgNW network ensures high conductivity. The resulting hybrid FTCFs displayed good photoelectric performance of 14.4 Ω/sq sheet resistance and 87.5% transmittance with enhanced stability, making them suitable for transparent heater applications.

4.4 Transparent conductive oxide (TCO)

The optoelectronic properties of TCO have been optimized for several decades, with typical low-temperature processed monolayer ITO achieving a sheet resistance of 40 Ω/sq and a transmittance of 85% [169]. Further enhancement of its conductivity often relies on hybridization with metallic materials. Among various approaches, the OMO structure enables synergistic optimization of optical and electrical performance through coupling between high-refractive-index oxide layers and an ultra-thin metal film. Ji et al. demonstrated a strategy for modulating the transmittance of an OMO configuration. Figure 6(a) illustrates an asymmetric OMO structure with its design parameters and reflection waves at various interfaces. The simulated average transmittance can be tuned across a wide range by adjusting the refractive index and thickness of the top oxide layer (Fig. 6(b)) [170]. By precisely controlling the thickness of metal and oxide layers (Fig. 6(c)), Zhang et al. fabricated an Mg and Ga codoped zinc oxide (MGZO)/Ag/MGZO transparent electrode with a resistance of 10 Ω/sq and 87% transmittance [171]. A key challenge in fabricating OMO structures is the growth of ultra-thin continuous metal layers. Huang et al. reported that introducing a seed layer and metal doping can effectively transfer the 3D island growth mode of Ag into a continuous 2D growth, enabling the formation of continuous ultra-thin Ag films, as illustrated in Fig. 6(d) [172, 173]. The inherent brittleness of ceramic oxides poses challenges to the mechanical stability of TCO-based films. As shown in Figs. 6(e) and 6(f), Cheon et al. utilized polytetrafluoroethylene (PTFE) to enhance interfacial adhesion and dissipate strain energy, thereby suppressing crack formation under bending stress [174]. The resulting PTFE/AgPdCu (APC)/indium zinc oxide (IZO) FTCFs exhibited a sheet resistance of 9.73 Ω/sq and outstanding flexibility, maintaining stable resistance after 10,000 bending cycles at a radius of 2 mm (Fig. 6(g)). Furthermore, metal atom diffusion at interfaces can lead to localized aggregation during aging or under thermal stress. This phenomenon represents another critical cause of OMO structural failure and warrants further investigation.

4.5 MXene

As a newly developed transparent conductive material, 2D transition metal carbide MXene has attracted significant attention. Via the traditional minimally intensive layer delamination (MILD) approach, $Ti_3C_2T_x$ typically exhibits an intrinsic conductivity of 5800 S/cm. With an optimized evaporated-nitrogen MILD synthesis, the conductivity can reach up to 24,000 S/cm [175]. The unique hydrophilic nature of MXenes enables surfactant-free aqueous ink formulation. This property addresses the dispersion challenges common to carbon-based materials and thereby significantly lowers processing costs. However, severe percolation problems were found in ultra-thin MXene films, as shown in Fig. 7(a) [176], making it difficult to simultaneously achieve high transmittance (> 90%) and low sheet resistance. To address this issue, Guo et al. synthesized large-sized $Ti_3C_2T_x$ flakes (12.2 μm) to reduce interflake resistance and constructed compact microstructures via blade coating [177]. The resulting films achieved 800 Ω/sq at a transmittance of 96.7%. Furthermore, by optimizing ink rheology and slot-die conditions, they produced large-area (approx. 250 cm^2) and uniform $Ti_3C_2T_x$ films with a sheet resistance of 498 Ω/sq at T = 94.5% [178]. The interconnected and highly aligned MXene nanosheets form compact conductive paths, effectively mitigating percolation problems. Nevertheless, previous literature has pointed out the oxidation issue of $Ti_3C_2T_x$ MXene, which easily degrades into insulating TiO_2 when exposed to

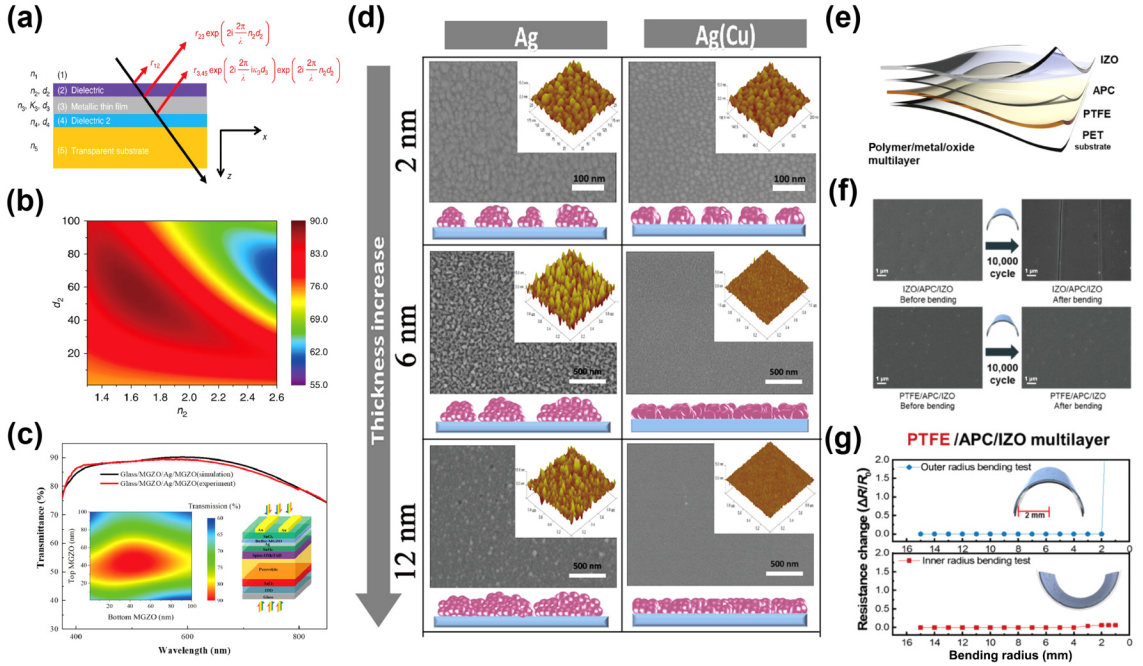

Figure 6 (a) Schematic diagram of OMO structure with design parameters and reflection waves at various interfaces. (b) Average transmittance versus refractive index (n_2) and thickness (d_2) of the top oxide layer. Reproduced with permission from Ref. [170], © Ji, C. G. et al. 2020. (c) Simulation and experimental results of transmission of MGZO/Ag/MGZO transparent electrode. Reproduced with permission from Ref. [171], © American Chemical Society 2021. (d) SEM and atomic force microscopy (AFM) images of pure Ag and Ag(Cu) thin films on glass substrates with increasing thickness. Conceptual diagrams representing the evolution of pure Ag and Ag(Cu) clusters with increasing thickness. Reproduced with permission from Ref. [172], © Elsevier B.V. 2018. (e) Schematics of the PTFE/APC/IZO FTCFs. (f) SEM images of the damage to the IZO/APC/IZO and PTFE/APC/IZO FTCFs after 10,000 bending cycles. (g) Critical bending radius of the PTFE/APC/IZO FTCFs. Reproduced with permission from Ref. [174], © Wiley-VCH GmbH 2024.

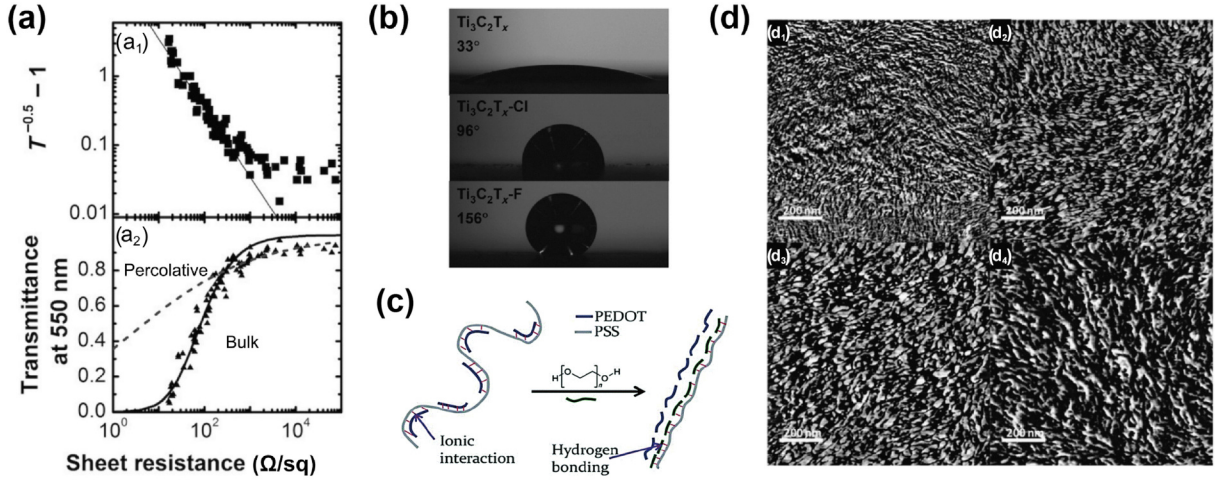

Figure 7 (a) Transmittance of $Ti_3C_2T_x$ films plotted as a function of sheet resistance. The solid line indicates the bulk-type conductivity behavior while the dashed line represents the percolative behavior. Reproduced with permission from Ref. [176], © WILEY-VCH Verlag GmbH & Co. KGaA, Weinheim 2016. (b) Water contact angle measurements for $Ti_3C_2T_x$, $Ti_3C_2T_x$-Cl, and $Ti_3C_2T_x$-F films. Reproduced with permission from Ref. [179], © American Chemical Society 2020. (c) Schematic illustration of the mechanism of conductivity enhancement of PEDOT:PSS with PEG. Reproduced with permission from Ref. [183], © The Royal Society of Chemistry 2013. (d) AFM phase images of PEDOT:PSS films with different Zonyl-FS300 concentrations. Reproduced with permission from Ref. [187], © WILEY-VCH Verlag GmbH & Co. KGaA, Weinheim 2012.

moisture and oxygen. Strategies such as surface chemical modification and hydrogen annealing have been employed to enhance the oxidation stability [179, 180]. For instance, as shown in Fig. 7(b), chloroalkylsilane and fluoroalkylsilane modifications on $Ti_3C_2T_x$ films (denoted as $Ti_3C_2T_x$-Cl and $Ti_3C_2T_x$-F) created a superhydrophobic surface, which effectively retards $Ti_3C_2T_x$ degradation under humid atmosphere [179]. Additionally, the mechanical flexibility of pure MXene films is limited by flake sliding and cracking during bending. Hybridization with AgNWs offers a viable solution, where AgNWs bridge the junctions between nanosheets, simultaneously lowering resistance and improving flexibility [150].

4.6 PEDOT:PSS

PEDOT:PSS is a highly conductive and transparent polymer widely employed as an electrode or charge-transport layer. It exhibits

excellent mechanical flexibility and ensures uniform current distribution. Composed of a conductive PEDOT phase and a dispersing PSS phase, the polymer is water-dispersible and can be readily processed into thin films via solution-based methods. As PSS is electrically insulating, the overall conductivity of PEDOT:PSS is intrinsically governed by the PSS content. For instance, the commercial CLEVIOS™ series exhibits conductivities ranging from 10^{-6} to 1 S/cm with varied PSS ratio [181]. To enhance the conductivity of PEDOT:PSS for FTCF applications, various secondary doping and post-treatment strategies have been developed. High-boiling-point polar solvents, such as dimethyl sulfoxide (DMSO), polyethylene glycol (PEG), glycerol, and sorbitol, are able to screen the coulombic interaction between $PEDOT^+$ and PSS^- via dipole interactions [182–185]. This process induces phase separation and linear orientation of the PEDOT chains, as shown in Fig. 7(c) [183]. Alternatively, strong acid treatments can convert ionic PSS^- into neutral PSSH and promote phase separation, eventually increasing the film conductivity by up to three orders of magnitude [186]. Vosgueritchian et al. reported PEDOT:PSS films achieving a sheet resistance of 46 Ω/sq at 82% transmittance by utilizing a combination of DMSO and a fluorosurfactant Zonyl-FS300 [187]. This performance enhancement was attributed to improved phase separation and the formation of more conductive PEDOT channels (Fig. 7(d)). Regarding environmental durability, the long-term stability of PEDOT:PSS is primarily compromised by its hygroscopic nature and intrinsic acidity. By incorporating waterborne acrylic resin into PEDOT:PSS, Jiang et al. successfully transformed the PEDOT:PSS film surface from hydrophilic to hydrophobic. Consequently, the air stability of solar cells fabricated with these electrodes was significantly improved [188]. Furthermore, PEDOT:PSS serves as an excellent matrix for composite FTCFs. Multiple studies have demonstrated that composites integrating silver nanoparticles (AgNPs), AgNWs, or MXene nanosheets with PEDOT:PSS exhibit superior conductivity and mechanical stability [189, 190].

5 Challenges in the industrialization and practical application of flexible transparent conductive films

5.1 Manufacturing readiness level evaluation

The gap between the academic breakthroughs and industrial application in FTCFs originates from a fundamental mismatch between laboratory-scale optimization and manufacturing readiness. First, academic research prioritizes maximizing the performance such as sheet resistance and transmittance, while neglecting the reproducibility in the fabrication process. In contrast, industrial production is yield-oriented, prioritizing batch-to-batch consistency through the strict control of factors such as raw materials, environmental conditions, and equipment parameters. Second, some laboratory-scale fabrication techniques are intrinsically non-scalable. For instance, transferring AgNWs deposition from spin-coating to R2R slot-die coating requires re-optimization of ink rheology and drying dynamics to accommodate continuous high-speed processing. Third, academic stability tests are generally conducted under isolated conditions, remaining limited understanding of degradation pathways involving multiple factors, such as electrochemical migration. In most cases, industrial applications require more complex and rigorous reliability test conditions. Finally, the economic feasibility of new FTCFs extends beyond raw material costs. The total industrial cost contains capital investment, operating expenditures, throughput, and yield losses. The cost assessments commonly used in academia often underestimate these systemic expenses.

To clearly assess the proximity of different FTCF technologies to practical applications, we applied the MRL framework to evaluate their industrial readiness [191]. Currently, metal mesh technology leads the field with an MRL of 9–10, having achieved full-scale application in large-sized touchscreens. Production lines for sub-3 μm metal mesh have already achieved stable yields, accompanied by a mature supply chain. AgNWs follow closely with an MRL of 8–9. As the haze and batch-to-batch variation issues have been largely resolved by leading suppliers, AgNWs are now transitioning to full-rate production for foldable smartphones. Meanwhile, OMO structures and CNTs are both positioned at MRL 7–8. For OMO with ultra-thin metal films, despite the mature sputtering process with seed layers, its widespread application is hindered by the high capital expenditure. Similarly, CNTs have only achieved low-rate initial production for limited applications in transparent heaters. In contrast, CVD graphene remains in the "Prototype to Pilot Line" stage with an MRL of 5–7, primarily restricted by its low cost-benefit ratio.

5.2 Matching practical requirements with the material performance

Based on the specific requirements of various applications outlined in Section 2.6, we can compare the performance metrics of different FTCFs to identify the most suitable candidates for specific application scenarios. A detailed comparison of key parameters for these FTCF materials in practical applications is summarized in Table 4. Taking capacitive touchscreens as an example, the most stringent requirement is a low sheet resistance below 10 Ω/sq, particularly as screen dimensions increase. Consequently, only metal-based FTCFs (including AgNWs, metal meshes, and ultra-thin metal films) can satisfy this conductivity standard. There are some differences among the three materials in terms of optical performance and intrinsic stability. AgNWs offer the highest transmittance of 91%–95% and superior flexibility but face challenges in optical haze and environmental stability issues. Metal meshes provide the best conductivity but require specialized designs to suppress moiré patterns. Ultra-thin metal films, typically used in

Table 4 Comparison of key parameters for different FTCF materials in practical applications

Materials	Sheet resistance	Transmittance	Cost	Key advantages	Key disadvantages
AgNWs	~ 10 Ω/sq	91%–95%	Medium	Flexibility, low resistance	Environmental stability, haze
Metal mesh	< 10 Ω/sq	85%–90%	Low	Low resistance	Moiré patterns
CNTs	100–500 Ω/sq	85%–90%	High	Flexibility, chemical stability	High resistance
Graphene	30–100 Ω/sq	> 90%	Very high	Thermal conductivity	Difficulty in transfer process
Ultra-thin metal film	~ 10 Ω/sq	80%–90%	Medium	Low resistance	Stability issues

OMO structures, exhibit low resistance. However, metal migration and aggregation remain significant stability challenges. In the current touchscreen market, metal meshes find their main application in tablets and notebooks, whereas AgNWs are preferred for smaller foldable smartphones. In contrast, carbon-based materials such as CNTs and graphene are generally unsuitable for capacitive touchscreens due to their relatively high sheet resistance.

The figure of merit (FOM) serves as a frequently used parameter in academic literature for assessing the combined optical and electrical performance of FTCFs. It provides a benchmark that facilitates the direct comparison of FTCFs across different material systems and structures. The classic Haacke's FOM (Φ_H) is defined by the transmittance (T) and sheet resistance (R_{sq}), expressed as [192]

$$\Phi_H = T^q / R_{sq} \quad (1)$$

where the exponent q is empirically assigned. Typically, q = 10 is adopted to reflect that transmittance exceeding 90% is sufficient for most applications. Alternatively, the ratio of optical and DC conductivity (σ_{opt}/σ_{DC}) is used as another definition of FOM. According to theory, the dependence of σ_{opt}/σ_{DC} on T and R_{sq} can be described by the formula [193]

$$T = \left(1 + \frac{Z_0}{2R_{sq}} \frac{\sigma_{opt}}{\sigma_{DC}}\right)^{-2} \quad (2)$$

where Z_0 represents the vacuum impedance. These two metrics effectively characterize the intrinsic optical and electrical properties of materials, where a higher FOM indicates superior transmittance at a particular sheet resistance. However, commercial devices generally impose rigid absolute thresholds for sheet resistance and transmittance, such as the 10 Ω/sq and 90% requirements for capacitive touchscreens discussed previously. While the FOM illustrates the trade-off trend between T and R_{sq}, it does not guarantee compliance with specific application criteria. Consequently, the FOM provides limited guidance for matching FTCF performance with practical requirements. Furthermore, the FOM fails to account for stability and scalability, which are often more critical factors for commercial applications.

5.3 Critical bottlenecks for metal-based FTCFs

The development of low-operation-voltage devices such as electrochromic devices requires extremely low sheet resistance to ensure large-area homogeneity and fast response. Similarly, emerging perovskite photovoltaics require ultrahigh conductivity for efficient charge collection. For applications with low sheet resistance below 10 Ω/sq, the use of conductive metals (especially silver and copper) is the only practically applicable pathway. Beyond chemical stability in harsh environments, electrochemical migration has recently been identified as a new degradation mechanism for metal-based FTCFs. Under forward bias in the presence of an electrolyte, metallic components within the FTCF can oxidize, dissolve into the electrolyte, and migrate as cations toward the cathode under the applied electric field. This process not only compromises the FTCF structure but also threatens other functional layers in the device. In the perovskite solar cells, researchers find that aged devices exhibit corrosion of Ag electrodes and diffusion of Ag^+ ions along cell edges. These Ag^+ ions react with iodide species released from perovskite decomposition, forming AgI at the interface and creating pinholes that lead to shunt paths [194]. Jeong et al. developed a hybrid FTCF consisting of a Cu grid embedded in polyimide and capped with a graphene layer, in which graphene serves as a barrier against both Cu electrochemical migration and halide diffusion [195]. Similarly, Domanski et al. demonstrated that inserting a Cr interlayer between the hole transport layer and the Au electrode effectively suppresses Au migration under operating conditions [196]. However, in light-emitting electrochemical cells, silver migration is not just a failure mechanism but can be intrinsically related to the p-doping process of the device. This necessitates complex designs that decouple hole injection from exciton formation to prevent degradation in stability [197]. In summary, suppressing electromigration requires comprehensive optimization based on the device's operational principles and architecture. The development of metal-based FTCFs with long-term operational stability still remains challenging.

Another key challenge for FTCFs in most applications is the tailoring of optical appearance with special focus on haze and color neutrality. Haze arises primarily from light scattering caused by structural features of the conductive material. In the case of AgNWs, the scattering intensity depends on nanowire diameter, and thus reducing the diameter contributes to lower optical haze. Yuan et al. synthesized ultra-thin AgNWs with the diameter down to 16 nm by using tetrabutyl ammonium dibromochloride (TBADBC) as the organic auxiliary [198]. The resulting FTCF exhibited a transmittance of 90.60%, a haze of 0.95%, and a sheet resistance of 110.8 Ω/sq. This result highlights the inherent trade-off between haze and conductivity. This trade-off can be further managed by increasing the number density of the thinner wires, which maintains the percolation network while reducing optical scattering [199]. Haze is also influenced by refractive index mismatches among the nanowires, air voids, and the substrate. Filling the voids with an index-matching material can effectively suppress scattering, enabling lower haze even in denser networks. In a study by Chae et al., a sandwich-like electrode was fabricated by deposition of GO films on both sides of the AgNW network [200]. The inhomogeneous nature of GO films lead to refractive index mismatch at the interfaces, leading to pronounced scattering within the electrode. By controlling GO deposition parameters, the transparency and haze levels of the electrode could be predictably tuned. Notably, different applications impose distinct requirements on electrode haze. For instance, LED devices and touch screens demand low haze to ensure display clarity, whereas photovoltaic devices benefit from higher haze for enhanced light trapping. Therefore, haze modulation must be optimized according to the specific application scenarios.

In display and transparent window applications, FTCFs must exhibit neutral color characteristics to ensure accurate color reproduction. Within the Commission Internationale de l'Éclairage (CIE) $L^*a^*b^*$ color space, a neutral color corresponds to a^* and b^* values close to zero. AgNW-based FTCFs typically exhibit a yellowish tint, characterized by a high positive b^* value. The yellow color arises principally from the surface plasmon resonance (SPR) of the silver nanowires, which has an absorption band in the 350–390 nm wavelength region [201]. To reduce b^* values and achieve color neutrality, several tuning and compensation strategies have been developed. Reducing the aspect ratio of AgNWs can induce a blue shift of the SPR absorption band out of the visible spectrum, thereby mitigating the yellow tint [202]. Cheon et al. demonstrated that a simple hydrazine treatment alters the chemical environment and dielectric constant around the AgNWs, shifting the plasmon absorption and reducing yellowness [203]. Similarly,

coating AgNWs with low-refractive-index materials such as CaF_2 and MgF_2 has been shown to effectively suppress yellowing. A more direct approach involves compensating the yellow tint using materials with a negative b^* value. For example, Kitamura et al. functionalized AgNWs with a polymer ligand (polyethylenimine-methoxy polyethylene glycol, PEI-mPEG) to adsorb an anionic blue dye (copper phthalocyanine-3,4,4″,4‴-tetrasulfonic acid tetrasodium salt, CuPTS) [204]. The complementary absorption in the UV–blue region resulted in a flatter absorption profile, leading to a more neutral color. Additionally, the intrinsic blue tint of conductive polymers like PEDOT:PSS can be utilized to counteract the yellowish appearance of AgNWs in AgNWs/PEDOT composite electrodes [205, 206].

6 Conclusion and perspectives

Materials are valuable only for being used. The present review discussed the major application fields of FTCFs and their specific requirements on FTCF properties, summarized the major large-area production pathways, and showcased recent major progress on materials and properties control. Achieving FTCFs with low sheet resistance and high transmittance remains the largest challenge, especially for large-area devices running under low voltage. Metal-containing films and/or structures are highly desired for such applications but face difficulties in both performance and stability. Furthermore, the transition from laboratory achievements to industrialization is often hindered by the cost of commercial substrates and the lack of specifically designed R2R systems. To bridge the gap between academic research and industrial application, concerted academia–industry collaboration is required to address the following critical challenges:

(1) Achieving low-temperature fabrication of metal-free FTCFs with extremely low sheet resistance to meet the stringent requirements of large-area perovskite solar cells (< 10 Ω/sq) and electrochromic devices (< 5 Ω/sq).

(2) Understanding the fundamental mechanisms of electrochemical migration in metal-based FTCFs and developing practical strategies to ensure long-term operational stability.

(3) Customizing FTCF materials and structures for electrochromic devices to satisfy the highly differentiated requirements of distinct terminals, such as architectural windows, automotive glass, and AR glasses.

(4) Discovering indispensable, market-driven applications for stretchable FTCFs to drive the establishment of standardized fabrication and characterization protocols.

Research and development on FTCFs, as one of the key materials for flexible electronics, will be speed up with focusing on key challenges in materials properties and considering large-area production and processing.

Data availability

All data needed to support the conclusions in the paper are presented in the manuscript. Additional data related to this paper may be requested from the corresponding author upon request.

Declaration of competing interest

All the contributing authors report no conflict of interests in this work.

Author contribution statement

Z. Q. Z.: Collecting references and writing Sections 3 and 4 of the manuscript. J. L.: Writing Section 2 of the manuscript. R. Q. T. and W. J. S.: Proposing the idea of this review, writing other sections of this review. All the authors have approved the final manuscript.

Use of AI statement

During the preparation of this work, the authors used Google Gemini 2.5 in order to improve grammar and writing style. After using this service, the authors reviewed and edited the content as needed and take full responsibility for the content of the publication.

References

[1] Meng, L. L.; Wang, W.; Xu, B. J.; Qin, J.; Zhang, K. J.; Liu, H. Solution-processed flexible transparent electrodes for printable electronics. *ACS Nano* **2023**, *17*, 4180–4192.

[2] Xu, Y. M.; Lin, Z. H.; Wei, W.; Hao, Y.; Liu, S. Z.; Ouyang, J. Y.; Chang, J. J. Recent progress of electrode materials for flexible perovskite solar cells. *Nanomicro Lett.* **2022**, *14*, 117.

[3] Li, D. D.; Lai, W. Y.; Zhang, Y. Z.; Huang, W. Printable transparent conductive films for flexible electronics. *Adv. Mater.* **2018**, *30*, 1704738.

[4] Kumar, S.; Seo, Y. Flexible transparent conductive electrodes: Unveiling growth mechanisms, material dimensions, fabrication methods, and design strategies. *Small Methods* **2024**, *8*, 2300908.

[5] Huang, S. Y.; Liu, Y. N.; Yang, F.; Wang, Y.; Yu, T.; Ma, D. L. Metal nanowires for transparent conductive electrodes in flexible chromatic devices: A review. *Environ. Chem. Lett.* **2022**, *20*, 3005–3037.

[6] Ghosh, A.; Hafnaoui, R.; Mesloub, A.; Elkhayat, K.; Albaqawy, G.; Alnaim, M. M.; Mayhoub, M. S. Active smart switchable glazing for smart city: A review. *J. Build. Eng.* **2024**, *84*, 108644.

[7] Lu, Q. C.; Lei, T. D.; Xu, J. G.; Qin, J. Principles, applications, and challenges of *E*-skin: A mini-review. *Chem. Eng. J.* **2025**, *521*, 166936.

[8] Papanastasiou, D. T.; Schultheiss, A.; Muñoz-Rojas, D.; Celle, C.; Carella, A.; Simonato, J. P.; Bellet, D. Transparent heaters: A review. *Adv. Funct. Mater.* **2020**, *30*, 1910225.

[9] Cheng, J. Y.; Li, C. B.; Xiong, Y. F.; Zhang, H. B.; Raza, H.; Ullah, S.; Wu, J. Y.; Zheng, G. P.; Cao, Q.; Zhang, D. Q. et al. Recent advances in design strategies and multifunctionality of flexible electromagnetic interference shielding materials. *Nanomicro Lett.* **2022**, *14*, 80.

[10] Wang, H. B.; Totaro, M.; Beccai, L. Toward perceptive soft robots: Progress and challenges. *Adv. Sci.* **2018**, *5*, 1800541.

[11] Mohamad, F.; Mat Teridi, M. A.; Chelvanathan, P.; Mohd Nasir, M. N.; Ibrahim, M. A. Recent development and challenges of flexible perovskite transparent conductive oxides in optoelectronic applications. *Mater. Sci. Semicond. Process.* **2025**, *196*, 109577.

[12] You, W. Q.; Liao, B. K.; Wan, S.; Guo, X. P. Research progress on the stability of transparent conductive films for silver nanowires. *Microelectron. Reliab.* **2024**, *156*, 115394.

[13] Du, J. H.; Pei, S. F.; Ma, L. P.; Cheng, H. M. 25th anniversary article: Carbon nanotube- and graphene-based transparent conductive films for optoelectronic devices. *Adv. Mater.* **2014**, *26*, 1958–1991.

[14] Meena, J. S.; Choi, S. B.; Jung, S. B.; Kim, J. W. Advances in silver nanowires-based composite electrodes: Materials processing, fabrication, and applications. *Adv. Mater. Technol.* **2023**, *8*, 2300602.

[15] Nguyen, V. H.; Papanastasiou, D. T.; Resende, J.; Bardet, L.; Sannicolo, T.; Jiménez, C.; Muñoz-Rojas, D.; Nguyen, N. D.; Bellet,

D. Advances in flexible metallic transparent electrodes. *Small* **2022**, *18*, 2106006.

[16] Chen, S.; Liang, L. S.; Zhang, Y. Q.; Lin, K. W.; Yang, M. N.; Zhu, L.; Yang, X. M.; Zang, L.; Lu, B. Y. PEDOT:PSS-based electronic materials: Preparation, performance tuning, processing, applications, and future prospect. *Prog. Polym. Sci.* **2025**, *166*, 101990.

[17] Du, J. H.; Tong, B.; Yuan, S. D.; Dai, N.; Liu, R.; Zhang, D. D.; Cheng, H. M.; Ren, W. C. Advances in flexible optoelectronics based on chemical vapor deposition-grown graphene. *Adv. Funct. Mater.* **2022**, *32*, 2203115.

[18] Cormia, R. L.; Fenn, J. B. Jr.; Memarian, H.; Ringer, G. Roll-to-roll coating of indium tin oxide—a status report. In *Proceedings of the 41st Annual Technical Conference of the Society of Vacuum Coaters*, Albuquerque, USA, 1998, pp 452–457.

[19] Luo, Y. F.; Abidian, M. R.; Ahn, J. H.; Akinwande, D.; Andrews, A. M.; Antonietti, M.; Bao, Z. N.; Berggren, M.; Berkey, C. A.; Bettinger, C. J. et al. Technology roadmap for flexible sensors. *ACS Nano* **2023**, *17*, 5211–5295.

[20] Nam, H.; Seol, K. H.; Lee, J.; Cho, H.; Jung, S. W. Review of capacitive touchscreen technologies: Overview, research trends, and machine learning approaches. *Sensors* **2021**, *21*, 4776.

[21] Alipoori, S.; Mehranpour, M. Advances in projected capacitive touch panels: Innovations in materials and fabrication techniques. *Metall. Mater. Data* **2025**, *3*, 107–114.

[22] Cho, S.; Kang, S.; Pandya, A.; Shanker, R.; Khan, Z.; Lee, Y.; Park, J.; Craig, S. L.; Ko, H. Large-area cross-aligned silver nanowire electrodes for flexible, transparent, and force-sensitive mechanochromic touch screens. *ACS Nano* **2017**, *11*, 4346–4357.

[23] Yu, H.; Tian, Y.; Dirican, M.; Fang, D. J.; Yan, C. Y.; Xie, J. Y.; Jia, D. M.; Liu, Y.; Li, C. X.; Cui, M. et al. Flexible, transparent and tough silver nanowire/nanocellulose electrodes for flexible touch screen panels. *Carbohydr. Polym.* **2021**, *273*, 118539.

[24] Franco, M.; Correia, V.; Marques, P.; Sousa, F.; Silva, R.; Figueiredo, B. R.; Bernardes, A.; Silva, R. P.; Lanceros-Mendez, S.; Costa, P. Environmentally friendly graphene-based conductive inks for multitouch capacitive sensing surfaces. *Adv. Mater. Interfaces* **2021**, *8*, 2100578.

[25] Guo, Z. J.; Li, X. L.; Li, N.; Liu, X. J.; Li, H. J.; Li, X. Z.; Wang, Y. X.; Liang, J. G.; Chen, Z. C. Multilayer directionally arranged silver nanowire networks for flexible transparent conductive films. *Phys. Chem. Chem. Phys.* **2023**, *25*, 14778–14785.

[26] Zhou, J. Y.; Zhang, H. C.; Wang, R.; Li, Z. H.; Li, H. K.; Duan, P. K.; Shang, S.; Zhang, Y. C.; Wang, Z. L.; Ge, W. S. et al. Hybrid additive manufacturing of ultra-fine high-resolution shell–core structured conductive mesh-based flexible transparent electrodes for flexible displays. *Virtual Phys. Prototyp.* **2023**, *18*, e2268602.

[27] Yuan, S. Q.; Fan, Z. B.; Wang, G. J.; Chai, Z. M.; Wang, T. Q.; Zhao, D. W.; Busnaina, A. A.; Lu, X. C. Fabrication of flexible and transparent metal mesh electrodes using surface energy-directed assembly process for touch screen panels and heaters. *Adv. Sci.* **2023**, *10*, 2304990.

[28] Zhou, Y.; Azumi, R. Carbon nanotube based transparent conductive films: Progress, challenges, and perspectives. *Sci. Technol. Adv. Mater.* **2016**, *17*, 493–516.

[29] Gaur, S. P.; Riyajuddin, S.; Kumar, S.; Ghosh, K. Large area graphene and their use as flexible touchscreens. In *Carbon Nanomaterial Electronics: Devices and Applications*. Hazra, A.; Goswami, R., Eds.; Springer: Singapore, 2021; pp 285–305.

[30] Nan, Z.; Wei, W.; Lin, Z. H.; Chang, J. J.; Hao, Y. Flexible nanocomposite conductors for electromagnetic interference shielding. *Nanomicro Lett.* **2023**, *15*, 172.

[31] Gupta, R.; Rao, K. D. M.; Kiruthika, S.; Kulkarni, G. U. Visibly transparent heaters. *ACS Appl. Mater. Interfaces* **2016**, *8*, 12559–12575.

[32] Liu, Q.; Tian, B.; Liang, J.; Wu, W. Recent advances in printed flexible heaters for portable and wearable thermal management. *Mater. Horiz.* **2021**, *8*, 1634–1656.

[33] Liu, M.; Xu, X. Y.; Zhao, T.; Zhou, H.; Yu, S. H.; Liu, H. Z.; Dong, X. Y. Preparation and properties of biodegradable AgNWs/chitosan super flexible transparent conductive films. *J. Mater. Sci. Mater. Electron.* **2025**, *36*, 1080.

[34] Lagrange, M.; Langley, D. P.; Giusti, G.; Jiménez, C.; Bréchet, Y.; Bellet, D. Optimization of silver nanowire-based transparent electrodes: Effects of density, size and thermal annealing. *Nanoscale* **2015**, *7*, 17410–17423.

[35] Sadeque, S.; Gong, Y.; Maize, K.; Ziabari, A. K.; Mohammed, A. M. S.; Shakouri, A.; Janes, D. B. Transient thermal response of hotspots in graphene-silver nanowire hybrid transparent conducting electrodes. *IEEE Trans. Nanotechnol.* **2018**, *17*, 276–284.

[36] Ning, W.; Wang, Z. H.; Liu, P.; Zhou, D. L.; Yang, S. Y.; Wang, J. P.; Li, Q. Q.; Fan, S. S.; Jiang, K. L. Multifunctional super-aligned carbon nanotube/polyimide composite film heaters and actuators. *Carbon* **2018**, *139*, 1136–1143.

[37] Chen, D. H.; Chua, M. H.; He, Q.; Zhu, Q.; Wang, X. Z.; Meng, H.; Xu, J. W.; Huang, W. Multifunctional electrochromic materials and devices recent advances and future potential. *Chem. Eng. J.* **2025**, *503*, 157820.

[38] Jeong, C. Y.; Kubota, T.; Tajima, K. Flexible electrochromic devices based on tungsten oxide and Prussian blue nanoparticles for automobile applications. *RSC Adv.* **2021**, *11*, 28614–28620.

[39] Duan, Z. J.; Wu, S. D.; Sun, H. L.; Lin, B. R.; Ding, P.; Cui, T.; To, J.; Zhang, X. Improvements in energy saving and thermal comfort for electric vehicles in summer through coupled electrochromic and radiative cooling smart windows. *Build. Simul.* **2024**, *17*, 1231–1251.

[40] Mesloub, A.; Ghosh, A.; Kolsi, L.; Alshenaifi, M. Polymer-dispersed liquid crystal (PDLC) smart switchable windows for less-energy hungry buildings and visual comfort in hot desert climate. *J. Build. Eng.* **2022**, *59*, 105101.

[41] Mesloub, A.; Ghosh, A.; Touahmia, M.; Albaqawy, G. A.; Alsolami, B. M.; Ahriz, A. Assessment of the overall energy performance of an SPD smart window in a hot desert climate. *Energy* **2022**, *252*, 124073.

[42] Zhang, S. L.; Peng, Y. T.; Zhao, J.; Fan, Z. J.; Ding, B.; Lee, J. Y.; Zhang, X. G.; Xuan, Y. M. Amorphous and porous tungsten oxide films for fast-switching dual-band electrochromic smart windows. *Adv. Opt. Mater.* **2023**, *11*, 2202115.

[43] Hao, T. T.; Wang, S.; Xu, H. B.; Zhang, X.; Xue, J. Y.; Liu, S. K.; Song, Y.; Li, Y.; Zhao, J. P. Highly robust, transparent, and conductive films based on AgNW-C nanowires for flexible smart windows. *Appl. Surf. Sci.* **2021**, *559*, 149846.

[44] Szymaniec, M.; Witkowski, F.; Brańko, F.; Białek, E.; Kaczmarski, J. Scalable fabrication of transparent conductive ITO thin films using chemical methods: Optimization of parameters and applications in functional glass technologies. *J. Alloys Compd.* **2025**, *1032*, 181195.

[45] Hu, Z. S.; Tang, X. Q.; Chen, X. L.; Huang, C. C.; Xu, W. Y.; Nie, S. H.; Zhao, Z. G.; Wu, X. Z.; Su, W. M.; Cui, Z. Ultra-low resistivity copper mesh as embedded current collector layer for inkjet-printed flexible electrochromic device realizing fast response and uniform coloration. *Adv. Mater. Technol.* **2023**, *8*, 2201037.

[46] Candeias, M. B.; Fernandes, T. V.; Falcão, B. P.; Cunha, A. F.; Cunha, J. M. V.; Barbosa, J.; Teixeira, J. P.; Fernandes, P. A.; Peres, M.; Lorenz, K. et al. Cu(In,Ga)Se_2-based solar cells for space applications: Proton irradiation and annealing recovery. *J. Mater. Sci.* **2023**, *58*, 16385–16401.

[47] Zhang, X.; Zhang, H.; Li, S. L.; Xiao, L. G.; Zhang, S. W.; Han, B.; Kang, J. J.; Zhou, H. Q. Development and application of blade-coating technique in organic solar cells. *Nano Res.* **2023**, *16*, 11571–11588.

[48] Dimngaihvungi, E.; Kumar Singh, A.; Pani, B.; Kumar Singh, A.; Singh, M. Polyimide impregnated silver nanowire-titanium oxide core–shell nanostructures as ultra-stable flexible transparent electrode for multiple applications. *J. Ind. Eng. Chem.* **2025**, *142*, 262–271.

[49] Zheng, X. J.; Wang, Y. M.; Chen, T. Y.; Kong, Y. B.; Wu, X. L.; Zhou, C.; Luo, Q.; Ma, C. Q.; Zuo, L. J.; Shi, M. M. et al. Realizing record efficiencies for ultra-thin organic photovoltaics through step-by-step optimizations of silver nanowire transparent electrodes. *FlexMat* **2024**, *1*, 221–233.

[50] Zhang, Q.; Nam, J. S.; Han, J. Y.; Datta, S.; Wei, N.; Ding, E. X.; Hussain, A.; Ahmad, S.; Skakalova, V.; Khan, A. T. et al. Large-diameter carbon nanotube transparent conductor overcoming performance–yield tradeoff. *Adv. Funct. Mater.* **2022**, *32*, 2103397.

[51] Passatorntaschakorn, W.; Khampa, W.; Musikpan, W.; Bhoomanee, C.; Ngamjarurojana, A.; Rimjaem, S.; Gardchareon, A.; Rodwihok, C.; Kim, H. S.; Khambunkoed, N. et al. A novel carbon electrode for up-scaling flexible perovskite solar cells. *Appl. Mater. Today* **2023**, *34*, 101895.

[52] Li, M. M.; Yue, Y.; Zhang, D.; Zhang, Y. J.; Wang, Y. C.; Zhang, X.; Wei, X. J.; Liu, H. P.; Zhou, W. Y. Lightweight and ultra-flexible perovskite solar cells with a "sandwich" perovskite layer based on graphene-carbon nanotube electrodes. *J. Mater. Chem. A* **2025**, *13*, 35547–35557.

[53] Lee, J.; Kim, M. S.; Jang, W.; Wang, D. H. Conductive PEDOT-dominant surface of transparent electrode patch via selective phase transfer for efficient flexible photoelectronic devices. *ACS Appl. Mater. Interfaces* **2024**, *16*, 38310–38323.

[54] Yuan, Z. Q.; Han, S. T.; Gao, W. C.; Pan, C. F. Flexible and stretchable strategies for electronic skins: Materials, structure, and integration. *ACS Appl. Electron. Mater.* **2022**, *4*, 1–26.

[55] Roy, A. C.; Kumar, N.; Subramanya, S. B.; Gupta, A.; Kumar, A.; Bid, A.; Venkataraman, V. Large-area 3D printable soft electronic skin for biomedical applications. *ACS Biomater. Sci. Eng.* **2022**, *8*, 5319–5328.

[56] Xu, C. H.; Solomon, S. A.; Gao, W. Artificial intelligence-powered electronic skin. *Nat. Mach. Intell.* **2023**, *5*, 1344–1355.

[57] Tian, C. H.; Khan, S. A.; Zhang, Z. Y.; Cui, X. J.; Zhang, H. L. Thermoelectric hydrogel electronic skin for passive multimodal physiological perception. *ACS Sens.* **2024**, *9*, 840–848.

[58] Liu, D. J.; Zhu, P. C.; Zhang, F. K.; Li, P. S.; Huang, W. H.; Li, C.; Han, N. N.; Mu, S. R.; Zhou, H.; Mao, Y. C. Intrinsically stretchable polymer semiconductor based electronic skin for multiple perceptions of force, temperature, and visible light. *Nano Res.* **2023**, *16*, 1196–1204.

[59] Tian, L. M.; Zimmerman, B.; Akhtar, A.; Yu, K. J.; Moore, M.; Wu, J.; Larsen, R. J.; Lee, J. W.; Li, J. H.; Liu, Y. H. et al. Large-area MRI-compatible epidermal electronic interfaces for prosthetic control and cognitive monitoring. *Nat. Biomed. Eng.* **2019**, *3*, 194–205.

[60] Shi, Y. H.; Zhang, B. C.; Zhao, J. Z.; Qin, J. H.; Bai, K.; Yu, J.; Zhang, X. H. A deformation mismatch strategy enables over 120% stretchability of encapsulated serpentine silicon strips for stretchable electronics. *FlexMat* **2024**, *1*, 150–159.

[61] Yang, S.; Cao, Y. J.; Han, K.; Guo, J. T.; Zheng, P. L.; Wang, L. Y.; Cheng, T.; Zhang, Y. Z.; Lai, W. Y. Stretchable transparent electrodes based on metal grid hybrids for skin-like multimodal sensing and flexible touch panel. *Nano Energy* **2025**, *139*, 110942.

[62] Sun, F. Y.; Xu, J. H.; Liu, T.; Li, F. F.; Poo, Y.; Zhang, Y. N.; Xiong, R. H.; Huang, C. B.; Fu, J. J. An autonomously ultrafast self-healing, highly colourless, tear-resistant and compliant elastomer tailored for transparent electromagnetic interference shielding films integrated in flexible and optical electronics. *Mater. Horiz.* **2021**, *8*, 3356–3367.

[63] Zhang, J.; Li, J. A.; Cheng, W.; Zhang, J. H.; Zhou, Z.; Sun, X. D.; Li, L. L.; Liang, J. G.; Shi, Y.; Pan, L. J. Challenges in materials and devices of electronic skin. *ACS Mater. Lett.* **2022**, *4*, 577–599.

[64] Sankar, S. D. Skin of the future?—Decoding electronic skin and a comprehensive review of the latest developments. *CosmoDerma* **2025**, *5*, 113.

[65] Li, L. X.; Han, L. J.; Hu, H. Q.; Zhang, R. Y. A review on polymers and their composites for flexible electronics. *Mater. Adv.* **2023**, *4*, 726–746.

[66] Crawford, R. J.; Martin, P. J. Chapter 4—Processing of plastics. In *Plastics Engineering*; 4th ed. Butterworth-Heinemann: Oxford, 2020; pp 279–409.

[67] Tao, J. S.; Wang, R. P.; Yu, H.; Chen, L. L.; Fang, D. J.; Tian, Y.; Xie, J. Y.; Jia, D. M.; Liu, H.; Wang, J. S. et al. Highly transparent, highly thermally stable nanocellulose/polymer hybrid substrates for flexible OLED devices. *ACS Appl. Mater. Interfaces* **2020**, *12*, 9701–9709.

[68] Mahdavipour, Z.; Karimi, M. A robust relation between mechanical modulus and thermal shrinkage force of PET filaments based on entropy stress. *Polymer* **2024**, *296*, 126781.

[69] Han, J. H.; Lee, K. H.; Park, S. J. Effects of plating conditions on thickness and surface roughness of electroless-plated Cu deposits. *Korean J. Met. Mater.* **2016**, *54*, 237–245.

[70] You, T. L.; Pan, Y. T.; Guo, G. X.; Yang, X. G.; Li, W. B.; Ma, C. F. Superior hard yet flexible, highly transparent, and scratch-repairable waterborne antiadhesive coatings enabled by multi-magnitude dynamic bonds synergy strategy. *Adv. Funct. Mater.* **2025**, *35*, 2420562.

[71] Jae, H.; Park, J.; Byun, J.; Chi, W. S.; Kim, J. H.; Jung, H. W.; Roh, D. Dual-cured organic-inorganic hard coating with high flexibility and transparency based on polysilsesquioxane and a functional polymer. *Prog. Org. Coat.* **2024**, *191*, 108416.

[72] De A. Freire, M. T.; Damant, A. P.; Castle, L.; Reyes, F. G. R. Thermal stability of polyethylene terephthalate (PET): Oligomer distribution and formation of volatiles. *Packag. Technol. Sci.* **1999**, *12*, 29–36.

[73] Huang, J. M.; Chu, P. P.; Chang, F. C. Conformational changes and molecular motion of poly(ethylene terephthalate) annealed above glass transition temperature. *Polymer* **2000**, *41*, 1741–1748.

[74] Gerlein, L. F.; Benavides-Guerrero, J. A.; Cloutier, S. G. Photonic post-processing of a multi-material transparent conductive electrode architecture for optoelectronic device integration. *RSC Adv.* **2024**, *14*, 4748–4758.

[75] Shi, L. R. Flexible transparent silver nanowires conductive films fabricated with spin-coating method. *Micro Nano Lett.* **2023**, *18*, e12151.

[76] Mochizuki, T.; Takigami, Y.; Kondo, T.; Okuzaki, H. Fabrication of flexible transparent electrodes using PEDOT:PSS and application to resistive touch screen panels. *J. Appl. Polym. Sci.* **2018**, *135*, 45972.

[77] Wu, X. Z.; Shao, S. S.; Chen, Z.; Cui, Z. Printed highly conductive Cu films with strong adhesion enabled by low-energy photonic sintering on low-Tg flexible plastic substrate. *Nanotechnology* **2017**, *28*, 035203.

[78] Hu, Y.; Zhang, H. D.; Pu, X. M.; Yang, L. P. Naphthyl copolyester with high glass transition temperatures: Tunable structure and performance. *ACS Appl. Polym. Mater.* **2024**, *6*, 14794–14801.

[79] Xu, Y. M.; Lin, Z. H.; Zhang, J. C.; Hao, Y.; Ouyang, J. Y.; Liu, S. Z.; Chang, J. J. Flexible perovskite solar cells: Material selection and structure design. *Appl. Phys. Rev.* **2022**, *9*, 021307.

[80] Jarvis, K. L.; Evans, P. J.; Triani, G. Influence of the polymeric substrate on the water permeation of alumina barrier films deposited by atomic layer deposition. *Surf. Coat. Technol.* **2018**, *337*, 44–52.

[81] Li, Y.; Wen, D.; Zhang, Y. H.; Lin, Y.; Cao, K.; Yang, F.; Chen, R. Highly-stable PEN as a gas-barrier substrate for flexible displays via atomic layer infiltration. *Dalton Trans.* **2021**, *50*, 16166–16175.

[82] Yuan, H.; Li, Q.; Yan, W. Q.; Zhang, Y. F.; Chen, L.; Pan, P.; Luo,

J.; Liao, B.; Ouyang, X. P. A novel and efficient technology of depositing Al_2O_3 film for OLEDs thin film encapsulation. *Vacuum* **2022**, *196*, 110741.

[83] Park, S.; Kim, L. H.; Jeong, Y. J.; Kim, K.; Park, M.; Baek, Y.; An, T. K.; Nam, S.; Jang, J.; Park, C. E. Reduced water vapor transmission rates of low-temperature-processed and sol-gel-derived titanium oxide thin films on flexible substrates. *Org. Electron.* **2016**, *36*, 133–139.

[84] Ni, H. J.; Liu, J. G.; Wang, Z. H.; Yang, S. Y. A review on colorless and optically transparent polyimide films: Chemistry, process and engineering applications. *J. Ind. Eng. Chem.* **2015**, *28*, 16–27.

[85] Zhang, X. X.; Li, X.; Li, L.; Shi, T. F. Effect of methyl trifluoride substitution on colorless transparency of polyimide: A DFT/TD-DFT study. *J. Mol. Liq.* **2024**, *411*, 125691.

[86] Su, C. X.; Liu, P. J.; Yue, J. Y.; Huan, H. J.; Yang, Z. H.; Yang, K.; Guo, H. Q.; Zhao, J. Y. High-transparency and colorless polyimide film prepared by inhibiting the formation of chromophores. *Polymers* **2022**, *14*, 4242.

[87] Ahn, C.; Kim, T. Y.; Hong, P. H.; Choi, S.; Lee, Y. J.; Kwon, H.; Jeon, H.; Ko, D. W.; Park, I.; Han, H. et al. Highly transparent, colorless optical film with outstanding mechanical strength and folding reliability using mismatched charge-transfer complex intensification. *Adv. Funct. Mater.* **2022**, *32*, 2111040.

[88] Yu, S. H.; Yang, P.; Wang, B.; Zhang, N.; Wu, C. High-temperature resistance of flexible transparent conductive films based on Ag@SnO_2 core–shell nanowires for 300 °C. *Mater. Lett.* **2022**, *328*, 133031.

[89] Yang, Z. H.; Guo, H. Q.; Kang, C. Q.; Gao, L. X. Synthesis and characterization of amide-bridged colorless polyimide films with low CTE and high optical performance for flexible OLED displays. *Polym. Chem.* **2021**, *12*, 5364–5376.

[90] Bae, J.; Ali, A.; Park, C.; Jang, J. High-performance, coplanar amorphous InGaZnO thin-film transistors by spray pyrolysis on polyimide substrate for low-cost manufacturing of foldable active-matrix organic light emitting diode display. *J. Soc. Inf. Disp.* **2023**, *31*, 308–315.

[91] Wen, Y.; Liu, H.; Yang, S. Y.; Fan, L. Transparent and conductive indium tin oxide/polyimide films prepared by high-temperature radio-frequency magnetron sputtering. *J. Appl. Polym. Sci.* **2015**, *132*, 42753.

[92] Kim, Y. N.; Lee, J.; Kim, Y. O.; Kim, J.; Han, H.; Jung, Y. C. Colorless polyimides with excellent optical transparency and self-healing properties based on multi-exchange dynamic network. *Appl. Mater. Today* **2021**, *25*, 101226.

[93] Shen, Y.; Feng, Z. C.; Zhang, H. Y. Study of indium tin oxide films deposited on colorless polyimide film by magnetron sputtering. *Mater. Des.* **2020**, *193*, 108809.

[94] Yun, H. W.; Choi, G. M.; Woo, H. K.; Oh, S. J.; Hong, S. H. Superhydrophobic, antireflective, flexible hard coatings with mechanically ultra-resilient moth-eye structure for foldable displays. *Curr. Appl. Phys.* **2020**, *20*, 1163–1170.

[95] Lee, Y.; Lee, H.; Im, H. G.; Jo, W.; Choi, G. M.; Kim, T. S.; Jang, J.; Bae, B. S. Transparent and flexible hybrid cover window film: Hard coating/substrate all-in-one composite film for reliable foldable display. *Composites* **2022**, *247*, 110336.

[96] Segawa, T.; Ikari, Y.; Ooba, N.; Kawakami, N.; Jiko, N.; Tao, H. New roll-to-roll sputtering system for wide film and application examples. *KOBELCO Technol. Rev.* **2016**, *34*, 44–51.

[97] Berg, S.; Nyberg, T. Fundamental understanding and modeling of reactive sputtering processes. *Thin Solid Films* **2005**, *476*, 215–230.

[98] Bishop, C. A. *Vacuum Deposition onto Webs, Films and Foils*; 2nd ed. William Andrew: Amsterdam, 2011.

[99] Bräuer, G.; Szyszka, B.; Vergöhl, M.; Bandorf, R. Magnetron sputtering—milestones of 30 years. *Vacuum* **2010**, *84*, 1354–1359.

[100] David, C.; Tinkham, B. P.; Prunici, P.; Panckow, A. Highly conductive and transparent ITO films deposited at low temperatures by pulsed DC magnetron sputtering from ceramic and metallic rotary targets. *Surf. Coat. Technol.* **2017**, *314*, 113–117.

[101] Lippens, P.; Frei, C. Tuning of ITO coating properties in the display industry: Selected topics. In *Proceedings of the 58th Annual Technical Conference of the Society of Vacuum Coaters*, Albuquerque, USA, 2015, pp 187–191.

[102] Robb, A. J.; Duca, Z. A.; White, N.; Woodell, P.; Ward, P. A. Influence of oxygen on the optical and electrical properties of magnetron-sputtered indium tin oxide thin films at ambient temperature. *Thin Solid Films* **2024**, *788*, 140152.

[103] Nakashima, K.; Kumahara, Y. Effect of tin oxide dispersion on nodule formation in ITO sputtering. *Vacuum* **2002**, *66*, 221–226.

[104] Liu, S. H.; Chen, J.; Sun, B. S.; Huai, Z. Y.; Xiong, F. D.; He, J. L. Evolution of microstructure of IGZO ceramic target during magnetron sputtering. *Ceram. Int.* **2022**, *48*, 7500–7511.

[105] Ahn, M. H.; Cho, E. S.; Kwon, S. J. Effect of the duty ratio on the indium tin oxide (ITO) film deposited by in-line pulsed DC magnetron sputtering method for resistive touch panel. *Appl. Surf. Sci.* **2011**, *258*, 1242–1248.

[106] Rogozin, A.; Vinnichenko, M.; Shevchenko, N.; Kolitsch, A.; Möller, W. Plasma influence on the properties and structure of indium tin oxide films produced by reactive middle frequency pulsed magnetron sputtering. *Thin Solid Films* **2006**, *496*, 197–204.

[107] Rogozin, A. I.; Vinnichenko, M. V.; Kolitsch, A.; Möller, W. Effect of deposition parameters on properties of ITO films prepared by reactive middle frequency pulsed dual magnetron sputtering. *J. Vac. Sci. Technol. A* **2004**, *22*, 349–355.

[108] Stowell, M.; Müller, J.; Ruske, M.; Lutz, M.; Linz, T. RF-superimposed DC and pulsed DC sputtering for deposition of transparent conductive oxides. *Thin Solid Films* **2007**, *515*, 7654–7657.

[109] Christie, D. J.; Walde, H. V.; Ash, T. J. Arc handling considerations for DC sputtering power supplies. In *Proceedings of the 48th Annual Technical Conference of the Society of Vacuum Coaters*, Albuquerque, USA, 2005, pp 39–43.

[110] Nishimura, E.; Ohkawa, H.; Song, P. K.; Shigesato, Y. Microstructures of ITO films deposited by d.c. magnetron sputtering with H_2O introduction. *Thin Solid Films* **2003**, *445*, 235–240.

[111] Boehme, M.; Charton, C. Properties of ITO on PET film in dependence on the coating conditions and thermal processing. *Surf. Coat. Technol.* **2005**, *200*, 932–935.

[112] Wang, M. X.; Wang, G. H.; Hu, M. Q.; Zhao, L.; Xu, X. H.; Xiao, J. H.; Gong, D. R.; Yu, C. Y.; Mo, L. B.; Diao, H. W. et al. Influence of unintentional H_2O introduction in sputtering chamber on ITO films and HJT solar cells. *Sol. Energy Mater. Sol. Cells* **2023**, *254*, 112274.

[113] Mattox, D. M. Chapter 3—the "good" vacuum (low pressure) processing environment. In *Handbook of Physical Vapor Deposition (PVD) Processing*. Mattox, D. M., Ed.; 2nd ed. William Andrew: Oxford, 2010; pp 73–145.

[114] Lee, S. M.; Koo, H. W.; Kim, T. W.; Kim, H. K. Asymmetric ITO/Ag/ZTO and ZTO/Ag/ITO anodes prepared by roll-to-roll sputtering for flexible organic light-emitting diodes. *Surf. Coat. Technol.* **2018**, *343*, 115–120.

[115] Seok, H. J.; Jang, H. W.; Lee, D. Y.; Son, B. G.; Kim, H. K. Roll-to-roll sputtered, indium-free ZnSnO/AgPdCu/ZnSnO multi-stacked electrodes for high performance flexible thin-film heaters and heat-shielding films. *J. Alloys Compd.* **2019**, *775*, 853–864.

[116] Cheng, Y. T.; Lu, T. L.; Hong, M. H.; Ho, J. J.; Chou, C. C.; Ho, J.; Hsieh, T. P. Evaluation of transparent ITO/nano-Ag/ITO electrode grown on flexible electrochromic devices by roll-to-roll sputtering technology. *Coatings* **2022**, *12*, 455.

[117] Dogan-Surmeier, S.; Gruber, F.; Bieder, S.; Schlenz, P.; Paulus, M.; Albers, C.; Schneider, E.; Thiering, N.; Maurer, C.; Tolan, M. et al.

Towards in-line real-time characterization of roll-to-roll produced ZTO/Ag/ITO thin films by hyperspectral imaging. *J. Phys. D: Appl. Phys.* **2023**, *56*, 365102.

[118] Park, J.; Shin, K.; Lee, C. Optimized design for anti-reflection coating process in roll-to-roll slot-die coating system. *Robot. Comput. Integr. Manuf.* **2014**, *30*, 432–441.

[119] Choi, S. H.; Shin, S.; Kim, W. Y.; Lee, J. M.; Park, S. R.; Kim, H.; Woo, K.; Kwon, S.; Fang, N. X.; Kim, S. et al. Scalable multistep roll-to-roll printing of multifunctional and robust reentrant microcavity surfaces via a wetting-induced process. *Adv. Mater.* **2025**, *37*, 2411064.

[120] Lee, M.; Parajuli, S.; Moon, H.; Song, R.; Lee, S.; Shrestha, S.; Park, J.; Yang, H.; Jung, Y.; Cho, G. et al. Characterization of silver nanoparticle inks toward stable roll-to-roll gravure printing. *Flex. Print. Electron.* **2022**, *7*, 014003.

[121] Jeong, T. J.; Yu, X. Q.; Harris, T. A. L. Scaled production of functionally gradient thin films using slot die coating on a roll-to-roll system. *ACS Appl. Mater. Interfaces* **2024**, *16*, 9264–9274.

[122] Wang, B. Y.; Lee, E. S.; Lim, D. S.; Kang, H. W.; Oh, Y. J. Roll-to-roll slot die production of 300 mm large area silver nanowire mesh films for flexible transparent electrodes. *RSC Adv.* **2017**, *7*, 7540–7546.

[123] Jeong, H.; Park, S.; Lee, J.; Won, P.; Ko, S. H.; Lee, D. Fabrication of transparent conductive film with flexible silver nanowires using roll-to-roll slot-die coating and calendering and its application to resistive touch panel. *Adv. Electron. Mater.* **2018**, *4*, 1800243.

[124] Shan, J. Q.; Hong, Y.; Wang, H. Y.; Cui, K. X.; Ding, J. B.; Guo, X. Z. Preparation and optoelectrical property of silver nanowire transparent conductive film via slot die coating. *Coatings* **2025**, *15*, 95.

[125] Kim, S.; Lee, J.; Lee, C. Computational fluid dynamics model for thickness and uniformity prediction of coating layer in slot-die process. *Int. J. Adv. Manuf. Technol.* **2019**, *104*, 2991–2997.

[126] Park, B. J.; Park, B. O.; Ryu, B. H.; Choi, Y. M.; Kwon, K. S.; Choi, H. J. Rheological properties of Ag suspended fluid for inkjet printing. *J. Appl. Phys.* **2010**, *108*, 102803.

[127] Wang, Y. H.; Wu, X. L.; Wang, K.; Lin, K. W.; Xie, H.; Zhang, X. B.; Li, J. Z. Novel insights into inkjet printed silver nanowires flexible transparent conductive films. *Int. J. Mol. Sci.* **2021**, *22*, 7719.

[128] Zhang, W. P.; Yang, J.; Knopf, G. K. Numerical simulation of solvent evaporation in a reactive silver ink droplet deposited on a heated substrate. *ACS Omega* **2023**, *8*, 38991–39003.

[129] Thayyil Raju, L.; Diddens, C.; Li, Y. X.; Marin, A.; van der Linden, M. N.; Zhang, X. H.; Lohse, D. Evaporation of a sessile colloidal water-glycerol droplet: Marangoni ring formation. *Langmuir* **2022**, *38*, 12082–12094.

[130] Devaraju, S.; Mohanty, A. K.; Won, D. H.; Paik, H. J. One-step fabrication of highly stable, durable, adhesion enhanced, flexible, transparent conducting films based on silver nanowires and neutralized PEDOT:PSS. *Mater. Adv.* **2023**, *4*, 1769–1776.

[131] Park, J.; Kang, H. J.; Gil, H.; Shin, K. H.; Kang, H. Roll-to-roll infrared and hot-air sintering of gravure-printed Ag layer based on *in situ* tension measuring and analysis. *J. Mater. Chem. C* **2016**, *4*, 8884–8888.

[132] Cherrington, M.; Claypole, T. C.; Deganello, D.; Mabbett, I.; Watson, T.; Worsley, D. Ultrafast near-infrared sintering of a slot-die coated nano-silver conducting ink. *J. Mater. Chem.* **2011**, *21*, 7562–7564.

[133] Yang, D. J.; Kim, S.; Sohn, H.; Moon, K. S.; Sim, W. H.; Jeong, H. M.; Shin, W. H. Effect of flash light sintering on silver nanowire electrode networks. *Materials* **2020**, *13*, 404.

[134] Kumar, D.; Stoichkov, V.; Brousseau, E.; Smith, G. C.; Kettle, J. High performing AgNW transparent conducting electrodes with a sheet resistance of 2.5 Ω Sq^{-1} based upon a roll-to-roll compatible post-processing technique. *Nanoscale* **2019**, *11*, 5760–5769.

[135] Yang, Y.; Ding, S.; Araki, T.; Jiu, J. T.; Sugahara, T.; Wang, J.; Vanfleteren, J.; Sekitani, T.; Suganuma, K. Facile fabrication of stretchable Ag nanowire/polyurethane electrodes using high intensity pulsed light. *Nano Res.* **2016**, *9*, 401–414.

[136] Xu, F.; Xu, W.; Mao, B. X.; Shen, W. F.; Yu, Y.; Tan, R. Q.; Song, W. J. Preparation and cold welding of silver nanowire based transparent electrodes with optical transmittances > 90% and sheet resistances < 10 ohm/sq. *J. Colloid Interface Sci.* **2018**, *512*, 208–218.

[137] Liu, J. C.; Lin, S.; Huang, K.; Jia, C.; Wang, Q. M.; Li, Z. W.; Song, J. N.; Liu, Z. L.; Wang, H. Y.; Lei, M. et al. A large-area AgNW-modified textile with high-performance electromagnetic interference shielding. *npj Flex. Electron.* **2020**, *4*, 10.

[138] Elechiguerra, J. L.; Larios-Lopez, L.; Liu, C.; Garcia-Gutierrez, D.; Camacho-Bragado, A.; Yacaman, M. J. Corrosion at the nanoscale: The case of silver nanowires and nanoparticles. *Chem. Mater.* **2005**, *17*, 6042–6052.

[139] Charvin, N.; Resende, J.; Papanastasiou, D. T.; Muñoz-Rojas, D.; Jiménez, C.; Nourdine, A.; Bellet, D.; Flandin, L. Dynamic degradation of metallic nanowire networks under electrical stress: A comparison between experiments and simulations. *Nanoscale Adv.* **2021**, *3*, 675–681.

[140] Lippens, P.; Muehlfeld, U. Indium tin oxide (ITO): Sputter deposition processes. In *Handbook of Visual Display Technology*. Chen, J. L.; Cranton, W.; Fihn, M., Eds.; Springer: Berlin, Heidelberg, 2012; pp 779–794.

[141] Chen, Z. B.; Yang, S. D.; Huang, J. H.; Gu, Y. F.; Huang, W. B.; Liu, S. Y.; Lin, Z. Q.; Zeng, Z. P.; Hu, Y. G.; Chen, Z. M. et al. Flexible, transparent and conductive metal mesh films with ultra-high FoM for stretchable heating and electromagnetic interference shielding. *Nanomicro Lett.* **2024**, *16*, 92.

[142] Chen, X. L.; Nie, S. H.; Guo, W. R.; Fei, F.; Su, W. M.; Gu, W. B.; Cui, Z. Printable high-aspect ratio and high-resolution Cu grid flexible transparent conductive film with figure of merit over 80 000. *Adv. Electron. Mater.* **2019**, *5*, 1800991.

[143] Yu, L. P.; Shearer, C.; Shapter, J. Recent development of carbon nanotube transparent conductive films. *Chem. Rev.* **2016**, *116*, 13413–13453.

[144] Ma, Y. J.; Zhi, L. J. Graphene-based transparent conductive films: Material systems, preparation and applications. *Small Methods* **2019**, *3*, 1800199.

[145] Yang, B. R.; Liu, G. S.; Han, S. J.; Cao, W.; Chen, H. J.; Lu, J. G.; Shieh, H. P. D. Hybrid effect of crossed alignment and multi-stacking structure on the percolation behavior of silver nanowire networks. *J. Disp. Technol.* **2015**, *11*, 625–629.

[146] Amirjani, A.; Marashi, P.; Fatmehsari, D. H. Effect of $AgNO_3$ addition rate on aspect ratio of $CuCl_2$-mediated synthesized silver nanowires using response surface methodology. *Colloids Surf. A* **2014**, *444*, 33–39.

[147] Lin, J. Y.; Hsueh, Y. L.; Huang, J. J.; Wu, J. R. Effect of silver nitrate concentration of silver nanowires synthesized using a polyol method and their application as transparent conductive films. *Thin Solid Films* **2015**, *584*, 243–247.

[148] Bleiji, Y.; Cordaro, A.; Tabernig, S. W.; Alarcón-Lladó, E. High aspect ratio silver nanogrids by bottom-up electrochemical growth as transparent electrode. *ACS Appl. Opt. Mater.* **2024**, *2*, 508–516.

[149] Li, D. D.; Lai, W. Y.; Feng, F.; Huang, W. Post-treatment of screen-printed silver nanowire networks for highly conductive flexible transparent films. *Adv. Mater. Interfaces* **2021**, *8*, 2100548.

[150] Jiang, W.; Lee, S.; Zhao, K. Y.; Lee, K.; Han, H.; Oh, J.; Lee, H.; Kim, H.; Koo, C. M.; Park, C. Flexible and transparent electrode of hybrid $Ti_3C_2T_X$ MXene-silver nanowires for high-performance quantum dot light-emitting diodes. *ACS Nano* **2022**, *16*, 9203–9213.

[151] Kim, D. H.; Yu, K. C.; Kim, Y.; Kim, J. W. Highly stretchable and mechanically stable transparent electrode based on composite of

silver nanowires and polyurethane-urea. *ACS Appl. Mater. Interfaces* **2015**, *7*, 15214–15222.
[152] Ye, C. H.; Gu, Y. J.; Wang, G. X.; Bi, L. L. Degradation mechanism of silver nanowire transparent conductive films: A review. *J. Inorg. Mater.* **2019**, *34*, 1257–1264.
[153] Kang, H.; Kim, J. S.; Choi, S. R.; Kim, Y. H.; Kim, D. H.; Kim, J. G.; Lee, T. W.; Cho, J. H. Electroplated core–shell nanowire network electrodes for highly efficient organic light-emitting diodes. *Nano Convergence* **2022**, *9*, 1.
[154] Jia, X. H.; Zhao, L.; Yang, P.; An, W. X.; Wang, Z. L.; Yu, S. H. Flexible transparent conductive films of Ag/Cr_2O_3 core–shell nanowires as electrodes for electroluminescent devices and heaters. *ACS Appl. Nano Mater.* **2023**, *6*, 16024–16033.
[155] Liu, G. S.; Xu, Y. W.; Kong, Y. F.; Wang, L.; Wang, J.; Xie, X.; Luo, Y. H.; Yang, B. R. Comprehensive stability improvement of silver nanowire networks via self-assembled mercapto inhibitors. *ACS Appl. Mater. Interfaces* **2018**, *10*, 37699–37708.
[156] Ding, Y. Y.; Zou, S.; Sun, H.; Su, X. D. Rayleigh analysis and numerical simulations of metal-mesh/transparent conducting oxide composite transparent electrode. *Acta Phys. Sin.* **2024**, *73*, 146801.
[157] Kelly, A. G.; Sheil, S.; Douglas-Henry, D. A.; Caffrey, E.; Gabbett, C.; Doolan, L.; Nicolosi, V.; Coleman, J. N. Transparent conductors printed from grids of highly conductive silver nanosheets. *ACS Appl. Mater. Interfaces* **2023**, *15*, 39864–39871.
[158] Jin, Y. X.; Cheng, Y. R.; Deng, D. Y.; Jiang, C. J.; Qi, T. K.; Yang, D. L.; Xiao, F. Site-selective growth of patterned silver grid networks as flexible transparent conductive film by using poly(dopamine) at room temperature. *ACS Appl. Mater. Interfaces* **2014**, *6*, 1447–1453.
[159] Lee, K. H.; Kim, S. M.; Jeong, H.; Pak, Y.; Song, H.; Park, J.; Lim, K. H.; Kim, J. H.; Kim, Y. S.; Ko, H. C. et al. All-solution-processed transparent thin film transistor and its application to liquid crystals driving. *Adv. Mater.* **2013**, *25*, 3209–3214.
[160] Li, H. K.; Zi, D. H.; Zhu, X. Y.; Zhang, H. C.; Tai, Y. P.; Wang, R.; Sun, L. F.; Zhang, Y. C.; Ge, W. S.; Huang, Y. Q. et al. Electric field driven printing of repeatable random metal meshes for flexible transparent electrodes. *Opt. Laser Technol.* **2023**, *157*, 108730.
[161] Križan, A.; Bardet, L.; Zimny, K.; Romanus, M.; Berthe, M.; Labrugère-Sarroste, C.; Bellet, D.; Tréguer-Delapierre, M. Oxidation-resistant Cu-based nanowire transparent electrodes activated by an exothermic reduction reaction. *ACS Nano* **2024**, *18*, 34902–34911.
[162] Chang, L.; Zhang, X. Q.; Ding, Y.; Liu, H. L.; Liu, M. Z.; Jiang, L. Ionogel/copper grid composites for high-performance, ultra-stable flexible transparent electrodes. *ACS Appl. Mater. Interfaces* **2018**, *10*, 29010–29018.
[163] Yang, H.; Bi, Y. G.; Wang, S. R.; Wang, C. F.; Wang, H. P.; Ye, G. D.; Feng, J. Ag-grid and Ag-nanowires hybrid transparent electrodes to improve performance of flexible organic light-emitting devices. *Photonics* **2025**, *12*, 272.
[164] Deng, B.; Liu, Z. F.; Peng, H. L. Toward mass production of CVD graphene films. *Adv. Mater.* **2019**, *31*, 1800996.
[165] Kobayashi, T.; Bando, M.; Kimura, N.; Shimizu, K.; Kadono, K.; Umezu, N.; Miyahara, K.; Hayazaki, S.; Nagai, S.; Mizuguchi, Y. et al. Production of a 100-m-long high-quality graphene transparent conductive film by roll-to-roll chemical vapor deposition and transfer process. *Appl. Phys. Lett.* **2013**, *102*, 023112.
[166] Liu, S. S.; Wu, Y. F.; Sun, Q. L.; Wu, S. Z.; Zhao, D. L. Preparation of conductive coating base on polymerizable carbon nanotubes modified by polythiophene derivatives. *Appl. Surf. Sci.* **2025**, *714*, 164423.
[167] Zhou, Y.; Tanaka, S.; Azumi, R. The use of acids in the exfoliation of carbon nanotubes and its application toward fabricating chemically stable and highly conducting transparent films. *Appl. Surf. Sci.* **2020**, *515*, 146027.
[168] Wang, P. C.; Jian, M. L.; Wu, M. Q.; Zhang, C.; Zhou, C. H.; Ling, X.; Zhang, J. H.; Yang, L. Q. Highly sandwich-structured silver nanowire hybrid transparent conductive films for flexible transparent heater applications. *Compos., Part A* **2022**, *159*, 106998.
[169] Yang, T.; Li, K.; Li, X. H.; Li, J.; Hu, C.; Fan, X. P.; Li, H. J.; Wang, R. X.; Liu, D. X.; Li, G. Q. Dual modulation of oxygen vacancies and dopants activation in sputtered ITO transparent conductive electrodes via low-temperature annealing. *J. Alloys Compd.* **2025**, *1044*, 184630.
[170] Ji, C. G.; Liu, D.; Zhang, C.; Guo, L. J. Ultrathin-metal-film-based transparent electrodes with relative transmittance surpassing 100%. *Nat. Commun.* **2020**, *11*, 3367.
[171] Zhang, Y. L.; Liu, Z.; Ji, C. G.; Chen, X. L.; Hou, G. F.; Li, Y. L.; Zhou, X.; Cui, X. H.; Yang, X. F.; Ren, C. C. et al. Low-temperature oxide/metal/oxide multilayer films as highly transparent conductive electrodes for optoelectronic devices. *ACS Appl. Energy Mater.* **2021**, *4*, 6553–6561.
[172] Huang, J. H.; Liu, X. H.; Lu, Y. H.; Zhou, Y. H.; Xu, J. J.; Li, J.; Wang, H. Q.; Fang, J. F.; Yang, Y.; Wang, W. Y. et al. Seed-layer-free growth of ultra-thin Ag transparent conductive films imparts flexibility to polymer solar cells. *Sol. Energy Mater. Sol. Cells* **2018**, *184*, 73–81.
[173] Huang, J. H.; Lu, Y. H.; Wu, W. X.; Li, J.; Zhang, X. P.; Zhu, C. T.; Yang, Y.; Xu, F.; Song, W. J. Amino-functionalized sub-40 nm ultrathin Ag/ZnO transparent electrodes for flexible polymer dispersed liquid crystal devices. *J. Appl. Phys.* **2017**, *122*, 195302.
[174] Cheon, H.; Park, S. M.; Lee, Y. S.; Kim, H. K. Flexible, conductive, and transparent polytetrafluoroethylene/AgPdCu/InZnO hybrid electrodes for transparent and flexible thin-film heaters. *Adv. Mater. Technol.* **2024**, *9*, 2401054.
[175] Zeraati, A. S.; Mirkhani, S. A.; Sun, P. C.; Naguib, M.; Braun, P. V.; Sundararaj, U. Improved synthesis of $Ti_3C_2T_x$ MXenes resulting in exceptional electrical conductivity, high synthesis yield, and enhanced capacitance. *Nanoscale* **2021**, *13*, 3572–3580.
[176] Dillon, A. D.; Ghidiu, M. J.; Krick, A. L.; Griggs, J.; May, S. J.; Gogotsi, Y.; Barsoum, M. W.; Fafarman, A. T. Highly conductive optical quality solution-processed films of 2D titanium carbide. *Adv. Funct. Mater.* **2016**, *26*, 4162–4168.
[177] Guo, T. Z.; Zhou, D.; Deng, S. G.; Jafarpour, M.; Avaro, J.; Neels, A.; Heier, J.; Zhang, C. F. Rational design of $Ti_3C_2T_x$ MXene inks for conductive, transparent films. *ACS Nano* **2023**, *17*, 3737–3749.
[178] Guo, T. Z.; Zhou, D.; Gao, M.; Deng, S. G.; Jafarpour, M.; Avaro, J.; Neels, A.; Hack, E.; Wang, J.; Heier, J. et al. Large-area smooth conductive films enabled by scalable slot-die coating of $Ti_3C_2T_x$ MXene aqueous inks. *Adv. Funct. Mater.* **2023**, *33*, 2213183.
[179] Chen, W. Y.; Lai, S. N.; Yen, C. C.; Jiang, X. F.; Peroulis, D.; Stanciu, L. A. Surface functionalization of $Ti_3C_2T_x$ MXene with highly reliable superhydrophobic protection for volatile organic compounds sensing. *ACS Nano* **2020**, *14*, 11490–11501.
[180] Lee, Y.; Kim, S. J.; Kim, Y. J.; Lim, Y.; Chae, Y.; Lee, B. J.; Kim, Y. T.; Han, H.; Gogotsi, Y.; Ahn, C. W. Oxidation-resistant titanium carbide MXene films. *J. Mater. Chem. A* **2020**, *8*, 573–581.
[181] Shahrim, N. A. A.; Ahmad, Z.; Azman, A. W.; Buys, Y. F.; Sarifuddin, N. Mechanisms for doped PEDOT:PSS electrical conductivity improvement. *Mater. Adv.* **2021**, *2*, 7118–7138.
[182] Lingstedt, L. V.; Ghittorelli, M.; Lu, H.; Koutsouras, D. A.; Marszalek, T.; Torricelli, F.; Crăciun, N. I.; Gkoupidenis, P.; Blom, P. W. M. Effect of DMSO solvent treatments on the performance of PEDOT:PSS based organic electrochemical transistors. *Adv. Electron. Mater.* **2019**, *5*, 1800804.
[183] Mengistie, D. A.; Wang, P. C.; Chu, C. W. Effect of molecular weight of additives on the conductivity of PEDOT:PSS and efficiency for ITO-free organic solar cells. *J. Mater. Chem. A* **2013**, *1*, 9907–9915.
[184] Yamaguchi, H.; Aizawa, K.; Chonan, Y.; Komiyama, T.; Aoyama, T.; Sakai, E.; Qiu, J. H.; Sato, N. Highly flexible and conductive

glycerol-doped PEDOT:PSS films prepared under an electric field. *J. Electron. Mater.* **2018**, *47*, 3370–3375.
[185] Khasim, S.; Pasha, A.; Roy, A. S.; Parveen, A.; Badi, N. Effect of secondary doping using sorbitol on structure and transport properties of PEDOT-PSS thin films. *J. Electron. Mater.* **2017**, *46*, 4439–4447.
[186] Li, Y. F.; Wen, R. J.; Li, P. C.; Fan, X. Metallic and low-work-function PEDOT:PSS cathodes for flexible organic solar cells exhibiting over 15% efficiency and high stability. *ACS Appl. Energy Mater.* **2022**, *5*, 7692–7700.
[187] Vosgueritchian, M.; Lipomi, D. J.; Bao, Z. N. Highly conductive and transparent PEDOT:PSS films with a fluorosurfactant for stretchable and flexible transparent electrodes. *Adv. Funct. Mater.* **2012**, *22*, 421–428.
[188] Jiang, L.; Zhou, Z.; Zhang, G. J.; Li, C. G.; Feng, Q. S.; Wei, Q. W.; Li, J. Y.; Wu, H. X.; Shi, Y.; Wang, J. et al. Waterborne acrylic resin-modified PEDOT:PSS as a hole-transporting layer for silicon/organic solar cells with improved efficiency and stability. *ACS Appl. Energy Mater.* **2024**, *7*, 3927–3936.
[189] Li, D. D.; Cui, J. J.; An, C. C.; Liu, Q. Y.; Xu, J.; Han, X.; Yang, S. C.; Lai, W. Y. Screen-printed PEDOT:PSS/Ag composite electrodes for high-performance paper-based supercapacitors. *Adv. Sustain. Syst.* **2025**, *9*, e00131.
[190] Li, D. D.; Liu, X.; Chen, X.; Lai, W. Y.; Huang, W. A simple strategy towards highly conductive silver-nanowire inks for screen-printed flexible transparent conductive films and wearable energy-storage devices. *Adv. Mater. Technol.* **2019**, *4*, 1900196.
[191] Office of the Secretary of Defense Manufacturing Technology Program, Joint Service/Industry MRL Working Group. *Manufacturing Readiness Level (MRL) Deskbook Version 2025* [Online]. https://www.dodmrl.com/MRL_Deskbook_2025.pdf (accessed Nov 18, 2025).
[192] Ellmer, K. Past achievements and future challenges in the development of optically transparent electrodes. *Nat. Photonics* **2012**, *6*, 809–817.
[193] De, S.; Coleman, J. N. Are there fundamental limitations on the sheet resistance and transmittance of thin graphene films. *ACS Nano* **2010**, *4*, 2713–2720.
[194] Ding, C. Z.; Yin, L.; Zhang, L. P.; Huang, R.; Fan, S. Z.; Luo, Q.; Lin, J.; Li, F. S.; Zhao, C.; Österbacka, R. et al. Revealing the mechanism behind the catastrophic failure of n-i-p type perovskite solar cells under operating conditions and how to suppress it. *Adv. Funct. Mater.* **2021**, *31*, 2103820.
[195] Jeong, G.; Koo, D.; Seo, J.; Jung, S.; Choi, Y.; Lee, J.; Park, H. Suppressed interdiffusion and degradation in flexible and transparent metal electrode-based perovskite solar cells with a graphene interlayer. *Nano Lett.* **2020**, *20*, 3718–3727.
[196] Domanski, K.; Correa-Baena, J. P.; Mine, N.; Nazeeruddin, M. K.; Abate, A.; Saliba, M.; Tress, W.; Hagfeldt, A.; Grätzel, M. Not all that glitters is gold: Metal-migration-induced degradation in perovskite solar cells. *ACS Nano* **2016**, *10*, 6306–6314.
[197] Youssef, K.; Li, Y.; O'Keeffe, S.; Li, L.; Pei, Q. B. Fundamentals of materials selection for light-emitting electrochemical cells. *Adv. Funct. Mater.* **2020**, *30*, 1909102.
[198] Yuan, X. M.; Yang, H. W.; Li, Y. X.; Li, Y.; Chao, Y. X.; Chen, J. L.; Chen, L. Synthesis of silver nanowires by using tetrabutyl ammonium dibromochloride as the auxiliary for low-haze flexible transparent conductive films. *Langmuir* **2019**, *35*, 11829–11835.
[199] Li, J.; Luo, J.; Liu, Y. Recent advances in silver nanowire-based transparent conductive films: From synthesis to applications. *Coatings* **2025**, *15*, 858.
[200] Chae, W. H.; Sannicolo, T.; Grossman, J. C. Double-sided graphene oxide encapsulated silver nanowire transparent electrode with improved chemical and electrical stability. *ACS Appl. Mater. Interfaces* **2020**, *12*, 17909–17920.
[201] Moores, A.; Goettmann, F. The plasmon band in noble metal nanoparticles: An introduction to theory and applications. *New J. Chem.* **2006**, *30*, 1121–1132.
[202] Ryu, S. M.; Nam, C. Shape-dependent optical properties of Ag nanowires synthesized using Pt and Cu seed materials. *Bull. Korean Chem. Soc.* **2020**, *41*, 184–189.
[203] Cheon, Y.; Nam, J.; Kim, C. S.; Jo, S. Reduced yellowing of silver nanowire transparent conductive electrodes by simple hydrazine treatment. *AIP Adv.* **2017**, *7*, 025215.
[204] Kitamura, S.; Iijima, M.; Tatami, J.; Fuke, T.; Hinotsu, T.; Sato, K. Polymer ligand design and surface modification of Ag nanowires toward color-tone-tunable transparent conductive films. *ACS Appl. Mater. Interfaces* **2021**, *13*, 13705–13713.
[205] Dcosta, J. V.; Ochoa, D.; Sanaur, S. Extensive properties investigation of AgNWs-PEDOT:PSS based transparent conductive electrode for ultraflexible organic photodetector applications. *Adv. Electron. Mater.* **2024**, *10*, 2300559.
[206] Noh, Y.; Cho, K. H. Piezoelectric dispenser printing and intense pulsed light sintering of AgNW/PEDOT:PSS hybrid transparent conductive films. *Nanotechnology* **2025**, *36*, 055301.